Experimental Investigations to Analyze Surface Contact Fatigue Wear by Using a Dynamic Response of the Roller Bearing System

Shashikant Pandey
PDPM IIITDM: PDPM Indian Institute of Information Technology Design and Manufacturing Jabalpur
Amarnath Muniyappa (amarnath.cmy@gmail.com)
PDPM IIITDM: PDPM Indian Institute of Information Technology Design and Manufacturing Jabalpur

Original Article

Keywords: Roller bearing, Lubricant film thickness, Wear, Vibrations

Posted Date: February 23rd, 2021

DOI: https://doi.org/10.21203/rs.3.rs-219458/v1

Experimental Investigations to analyze surface contact fatigue wear by using a dynamic response of the roller bearing system

Shashikant Pandey, M. Amarnath

Machine Dynamics and Tribology Laboratory, Department Mechanical Engineering, PDPM Indian Institute of Information Technology Design and Manufacturing Jabalpur, M.P. India 482005

Corresponding author

M Amarnath *

Department of Mechanical Engineering

Indian Institute of Information Technology Design and Manufacturing, Jabalpur 482005, India

Tel: 0761-2794417 Email: amarnath.cmy@gmail.com

Abstract

Bearings are used to reduce friction between two rolling /sliding members of the machines. Under normal operating conditions, an increase in the fatigue load cycles on the bearing contact surfaces results in surface defects viz. micro pitting, macro pitting, spalling and scuffing, thereby causing lubricant degradation. Hence, to maintain a better operating performance of rotating machines, it is essential to keep track of operating parameters. This paper describes the results of experimental investigations carried out to assess wear propagation on bearing contact surfaces using tribological and vibration parameters. Results obtained from experimental investigations provide a good correlation between the increase in surface fatigue wear and corresponding effects on transition in lubrication regimes, increased vibration levels, variations in rheological properties of lubricant and wear mechanisms developed on the contact surfaces of the roller bearing. The proposed approach can be used as a promising tool to assess incipient faults developed in roller bearing.

Keywords: Roller bearing, Lubricant film thickness, Wear, Vibrations

Introduction

The roller element bearing is an essential component in various power transmission devices and drives. Grease and oil are the most commonly used lubricants in the rolling element bearings. It forms a lubricant film between the races in the rolling element bearing, serves as a coolant, flushes wear debris and provide corrosion resistance. Degradation of lubricant is the primary reason for bearing failure if the lubricant film between rolling element contacts collapses for any length of time, excessive wear and heating occur on bearing contact surfaces, thereby causing various wear mechanisms viz. abrasive wear, adhesive wear, corrosive wear, etc. which eventually lead to

bearing failure. The unforeseen bearing failures result in substantial time and economic losses in the industrial plant [1].

In the last decade, researchers were keen on investigating the mechanisms of bearing failure and their characteristics to obtain diagnostic information of damage at the early stage. Two methods are widely used to study the characteristics of bearing failures, run to failure tests and simulation of localized defects on bearing components. Localized defects are simulated on the bearing surface by scratching, acid etching, or by using electric discharge machining [2,3]. Rolling element bearing defects are divided into two categories; distributed defects and localize faults. Defects such as an increase in roughness and waviness between contact surfaces and off size of a rolling element are considered distributed defects caused due to improper lubrication, misalignment of bearing, or manufacturing defects. Localized defects include cracks, pits, spall, etc. on the bearing component surfaces [4]. In general, the fault assessment in a rolling/sliding contact machine element is carried out by considering two basic approaches. The first approach includes the estimation of specific film thickness, wear particle morphology studies and oil degradation analysis, etc. The second approach considers the measurement and analysis of vibration, sound and acoustic emission signal, etc.[5,6].

Yusof et al. [7] carried out experiments to assess surface fatigue wear propagated on unlubricated and grease-lubricated bearings. Results obtained from experiments highlighted the importance of surface roughness and surface waviness parameters to evaluate the severity of wear propagation on the rolling contacts. Authors observed that wear severity developed on the inner race surface is higher than degradation appeared on the other rolling component surfaces.

Further, vibration signal analysis was also used in conjunction with lubricant film thickness analysis to assess bearing faults. Karacay and Akturk [8] conducted experimental studies to detect

incipient faults in a ball bearing. Experiments were conducted on the overhang rotor system; the test bearing was one among the support bearing. The authors have considered traditional statistical parameters to diagnose defect severity. Results obtained in this experimental work conclude that defects are formed on the inner race of the ball bearing at the initial stage.

Ueda and Mitamura [9] studied the mechanism of dent-initiated flaking on the inner race and its effect on bearing life under contaminant lubrication conditions. Experimental observations indicated that the dents appeared on a raceway significantly influence the bearing life. Al-Ghamd [10] conducted an experimental study to compare the effectiveness of acoustic emission (AE) and vibration signal analysis methods for bearing defect identification and defect size estimation. Authors have established a relationship between the AE burst duration and the defect dimensions; the AE sensor provided better diagnostic information than a vibration sensor. Koulocheris et al. [11] have explored the negative impacts of contaminants in grease lubrication on the wear and fatigue life of roller bearing. The bearing fault assessment was carried out using vibration signals in conjunction with wear particle morphology and wear mechanism analysis; the results showed the possible origin of wear mechanisms. The micrographs showed oxidization marks, dull finishing and micro pitting on the rolling surfaces.

Zong et al. [12] proposed a method to study the fatigue properties and to predict the remaining useful life of a slewing bearing used in a wind turbine generator. An experimental test rig was developed to conduct accelerated fatigue life tests, reflecting the actual state of slewing bearing employed to realistic working conditions in wind power generation plants. Serrato et al. [13] conducted experiments on roller bearing to investigate the effect of lubricant viscosity on the vibration levels of the roller bearing system. The authors found that temperature and RMS values of vibration signals tend to increase and stabilize with an increase in operating time. The relation

between specific film thickness (λ) and RMS values of bearing vibration signals showed a good agreement with the standard Stribeck curve.

Effect of transition in lubrication regimes in wear mechanisms and dynamic response in roller bearing system

The primary function of the lubricant in roller element bearing is to form a thick lubricant film, which separates the rolling surfaces of the bearing to minimize friction and wear. As a result, the operating life of bearing prolongs to serve desired industrial applications [1]. In general, almost all lubricated machine elements operate in three-lubrication regimes viz. hydrodynamic (HL), elastohydrodynamic (EHL) and boundary lubrication (BL) systems. Mixed lubrication indicates the intermediate regime between EHL and boundary lubrication.

Figure 1 depicts the Stribeck curve, which summarizes variations of three lubrication regimes and the friction characteristics of the lubricated machine elements. A change in the coefficient of friction depends on dimensionless specific film thickness parameter represented by 'λ' higher values ($\lambda > 3$) are associated with full film lubrication whereas lower values ($\lambda<1<3$) and ($\lambda<1$) represent Mixed and BL regime respectively [13-15].

The variation in operating conditions and an increase in surface roughness between contact surface results transition in the lubrication regime from HL to EHL. In elastohydrodynamic lubrication, some elastic deformation occurs between metal contact surfaces due to high contact pressure. The fluid film formed between the two contacting surfaces supports the load in the HL and EHL contacts. The surface fatigue is the primary reason for the appearance of wear on contacting surfaces. In the EHL regime, machine elements undergo mild wear on their contact surfaces. The bearing vibrations generated in the EHL regime include rotational vibration and periodic impacts, as shown in Figure 1, which appear due to defects such as micro and macro pittings developed on

the bearing contact surfaces. In the BL regime, oil wets only to the contact surfaces; hence the hydrodynamic action is too weak for separating the contact surfaces from each other. The load applied is carried by metal to metal contacts and boundary film formed between metallic surfaces. In this regime, the lubricant properties, chemical composition and surface chemistry of contact materials play a significant role in serving the intended purpose of lubrication [17]. The direct metal-to-metal contact conditions in bearing result in wear propagation on the rolling contact surfaces, boundary lubricated contacts lack damping effect and act as vibration sources. The vibration signals generated in the BL regime encompass higher amplitudes in temporal plots, as shown in Figure 1 [18].

Formation of EHL and development of failure mechanism

In general, EHL lubrication is found in non-conformal contacts such as gears, cams and point/ line contact bearings. In the EHL regime, the physical interaction takes place between the lubricant and the contacting bodies. The oil film thickness in the EHL regime of the roller bearing is slightly higher than the combined surface roughness of the rolling element and the raceways [19]. Figure 2 represents the formation of the EHL regime in the rolling element bearing. The enlarged view of two matting cylinders, i.e., inner race and roller, highlights the interaction between the lubricant and rolling bodies. A thick line represents the EHL pressure; the dotted line indicates Hertzian contact pressure and a thick red line highlights the profile of film thickness in the EHL regime. Lubricant entrainment is from left to right, and the lubricant inlet is assumed to be fully flooded, which results in hydrodynamic pressure in the rolling contacts. The EHL pressure gradually increases in the inlet region and reaches a maximum value at the center. The central zone of the contact is known as a Hartzain contact region; the EHL pressure profile is similar to dry rolling contact. However, the Hertzian pressure profile consists of a pressure spike towards the outlet. In

the Hertzian region, the opposing surfaces are separated by uniform film thickness, often referred to as central film thickness, 'h_c' as shown in Figure 2 (b) [20].

Under high pressure, the lubricant viscosity increases exponentially in the Hertzian contact zone; hence, lubricant fails to squeeze out from the contact surfaces. As the lubricant flow towards the exit, the higher viscosity of lubricant causes the sharper decline to the ambient magnitude of lubricant pressure, this zone is known as the cavitation region. In this region, the lubricant film does not exist; however, constriction is formed near the exit of the contact. The film thickness present at the contraction is called minimum film thickness 'h_{min}', as shown in Figure 2 (b). The minimum film thickness value is necessary to assess operating conditions in all lubricated rolling/ sliding contact machine elements [21].

During the run-in wear period, the wear rate is high; however, an increase in load cycles results in smoother contact surfaces, thereby causing a gradual reduction in wear rate. After the run-in wear period, a steady low wear rate persists in the operational life of rolling contact machine elements. The wear rate again rises as the operating time prolongs in conjunction with the fatigue load cycles [22,23]. The most common wear mechanism in cylindrical roller bearing is rolling contact fatigue, which results from cyclic loading on contact surfaces. Rolling contact fatigue leads to surface cracks, which results in the formation of microscale pitting on bearing contact surfaces. On the other hand, rolling contact fatigue also triggers subsurface cracks; these subsurface cracks-initiated spalling are the dominant cause of bearing failure [15,24,25].

Assessment of lubricant film thickness in rolling element bearing

The hydrodynamic and elastohydrodynamic lubrication regimes play a significant role in preventing direct metal-to-metal contact between two rolling contact machine elements. The primary functions of lubrication are to minimize friction, wear, abnormal vibration levels and heat

generated by rolling/ sliding contact surfaces. The lubricant film provides a separation between the races and the roller elements in the bearing. Reduction in the lubricant film thickness is the root cause of various bearing failure modes [6,18]. Hence, it is essential to measure, model, or estimate the film thickness with a high degree of accuracy under actual operating conditions of machine elements.

Based on numerical simulations and experimental results, Dowson and Higginson [16,26] established an empirical formula to determine the minimum film thickness at the outlet of lubricated roller contact surfaces under fully flooded, isothermal conditions. Pan and Hamrock [7] modified Dowson's formula to estimate lubricant film thickness for line contact bearing, which is given by the equation (1)

$$\frac{h_{\min}}{R_x} = 1.714 U_r^{0.694} G^{0.568} W^{-0.128} \quad (1)$$

Where U_r, G, W, R_x are dimensionless speed, material, load parameters and equivalent radius respectively. Expressions for the estimation of film thickness under the isothermal and fully flooded conditions are only valid for relatively lower speed and load conditions.

Importance of correction factors in lubricant film thickness analysis

The accurate estimation of lubricant film thickness in both conformal and non-conformal contacts is essential for the effective assessment of their operating conditions. Equation (1) discussed in the previous section is used to estimate fluid film thickness in the cylindrical roller bearing, which relies on the assumption of the isothermal condition, Newtonian fluid model and adequate supply of lubricant. According to studies conducted [7,16,27], equation (1) overestimates the fluid film thickness in the rolling/sliding contact machine element. Assumptions in equation (1) differ from

the actual operating conditions in the non-conformal EHL contacts. In the Hertzian contact region, the lubricant temperature is not constant; lubricant exhibits non-Newtonian properties and inadequate lubricant supply exists between contact surfaces. To overcome the aforementioned limitations, the researchers put their efforts into modeling / predicting the fluid film thickness more accurately by introducing various correction factors closer to the actual operating conditions. The important correction factors to be considered for accurate estimation of lubricant film thickness are thermal and starvation correction factors [16,28,29].

Thermal correction factor

The empirical expressions used in the lubricant film thickness analysis overestimated the film thickness, valid for low speed and load operating conditions. At higher speeds and slip ratios, the film thickness analysis requires correction due to viscous heating of lubricant at the contact zone. Hsu and Lee [30] have developed an empirical formula by considering the thermal correction factor ($C_{thermal}$), which is given in equation (2).

$$C_{thermal} = (1 + 0.0766G^{0.687}W^{0.447}L^{0.527}e^{0.8755S})^{-1} \quad (2)$$

L is the thermal loading parameter is given by

$$L = \frac{\eta_0 \gamma u^2}{k} \quad (3)$$

Starvation correction factor

Dowson's equation used to estimate lubricant film thickness assumes an adequate lubricant supply in the contact zone. However, in the actual conditions, the lubricant volume entering the contact zone is insufficient to develop a full film lubricant film between the contact surfaces, causing starvation. The equation for starvation factor $C_{stravation}$ is given in equation (4) [31].

$$C_{stravation} = 1\text{-}\exp\left[-1.68005\,\varphi^{0.8315} + 0.2610137\,\varphi^{1.558} - 0.016146\,\varphi^{2.296}\right] \quad (4)$$

Where $\varphi = \frac{x_0}{b}\left(\frac{b^2}{2h_e R}\right)^{2/3}$

Hence, the modified film thickness is given in equation (5), which considers thermal and starvation factors.

$$h^*_{\min} = C_{stravation} \times C_{thermal} \times h_{\min} \quad (5)$$

The specific film thickness (λ) is used to define the lubrication regimes in the bearing system [7,27]. It is also known as effective film thickness, which considers the effect of surface roughness values of contacting bodies is given by equation (6).

$$\lambda = \frac{h_{\min}}{\sqrt{R^2{}_{q_1} + R^2{}_{q_2}}} \quad (6)$$

Where Rq_1, Rq_2 are root mean square values of the surface roughness of inner race and roller surfaces. If $\lambda > 3$, it indicates bearing is operating in elastohydrodynamic lubrication or hydrodynamic lubrication regime. In this regime, inner race and rollers are fully separated through a thick lubricant film. If λ is between $1 < \lambda < 3$, then the lubrication regime obtain is known as the mixed lubrication regime, in which contact surfaces are partially separated by a lubricant film and in some points, there is metal-to-metal contact. The lubrication regime transition occurs from EHL to BL due to a decrease in λ values, generally $\lambda \leq 1$. The boundary lubrication regime results in direct metal-to-metal contact, causing severe wear defects on the bearing contact surfaces [14].

Rheology of rolling lubricating oil

Under the normal load, slow speed and low bearing temperature, the shear stress is low; lubricant in the roller bearing behaves like a Newtonian fluid where the shear stress is directly proportional

to shear strain. The multi-grade lubricating oil is a non-Newtonian fluid, in which there is a reduction in viscosity under high shear stress; this loss can be temporary or permanent. A drastic reduction in viscosity under high shear stress occurs due to the elongation and orientation of polymer molecules in the flow direction. In the EHL contact, the lubricant pressure is very high, about one GPa; with an increase in the load and velocity, the temperature in the bearing increases, which causes a reduction in the viscosity of the lubricant. As the shear stress in the oil increases, large molecules of multi-grade additives tend to break into smaller pieces. The breakdown of additive molecules causes a permanent viscosity loss in the lubricating oil. Loss of viscosity under high shear stress can be attributed to the mechanical degradation of lubricant [32,33].

A flow curve is a graphical representation, which describes the dynamic viscosity as a function of the shear rate, as shown in Figure 3. The flow curve of the lubricating oil has been divided into three zones. In the first zone, lubricating oil possesses a Newtonian behavior, where the apparent viscosity does not depend on the shear rate. Further, an increase in shear rate causes shear thinning and reduction in the dynamic viscosity in the second zone, as shown in Figure 3. As the shear rate increases, shear-thinning becomes less significant; as shown in the third zone, the dynamic viscosity becomes constant with a further increase in the shear rate. This third region is also called the second Newtonian plateau, where the shear rate is very high [32,34,35].

Vibration signal analysis

In general, vibration signals are acquired using displacement, velocity and acceleration sensors; among these sensors, accelerometers are widely used to detect faults in rotating machinery. These sensors possess the best amplitude response in the frequency range up to 20 kHz. Fault related features extracted from time and frequency domain signals provide diagnostic information to detect fault severity in the bearings. The time-domain analysis of vibration signals is the most

popular technique used in the classification of bearing faults. The statistical features viz. mean, standard deviation, root mean square, kurtosis, skewness extracted from the measured vibration signals are used to detect defects in a bearing. The most commonly used statistical parameters of vibration signals are given below [8,37,38].

Root mean square (RMS): The root mean square (RMS) is defined as the variance of the signal magnitude.

$$X_{RMS} = \sqrt{\frac{1}{N}\sum_{n=1}^{N} X^2(n)} \tag{7}$$

Crest Factor (C_f): The crest factor is obtained by dividing the maximum peak value of the vibration signal by its RMS value.

$$C_f = \frac{X}{X_{RMS}} \tag{8}$$

Peak-to-Peak value (X_{pp}): This value gives the difference between the maximum positive peak amplitude and the maximum negative peak amplitude.

$$X_{pp} = x_{\max}(t) - x_{\min}(t) \tag{9}$$

Kurtosis: Kurtosis indicates the flatness or the spikiness of the signal. Its value is very low for normal condition of a bearing and high for the faulty condition of the bearing due to the spiky nature of the signal.

$$Kurtosis = \frac{1}{N}\sum_{n=1}^{N} \frac{(x(n)-\bar{x})^4}{\left[\frac{1}{N}\sum_{n=1}^{N}(x(n)-\bar{x})^2\right]^2} \tag{10}$$

The frequency-domain method is another technique used for fault detection in bearing. Defects developed on the bearing contact surfaces produce various characteristic frequencies in the frequency spectrum, which reveal the location of faults on bearing contact surfaces. Fast Fourier Transform (FFT) is a widely used method to plot the frequency spectrum, highlighting defect

frequencies, sub-harmonics and super-harmonics. The characteristic frequencies of a bearing are given in the following equations [8,7,36].

Ball Pass Frequency-Outer Race (BPFO)

$$BPFO = \frac{n}{2} \times \frac{N_r}{60} \times \left[1 - \left(\frac{d}{D} \right) COS\beta \right] \text{ Hz} \quad (11)$$

Ball Pass Frequency-Inner Race (BPFI)

$$BPFI = \frac{n}{2} \times \frac{N_r}{60} \times \left[1 + \left(\frac{d}{D} \right) COS\beta \right] \text{ Hz} \quad (12)$$

Rolling Element Frequency

$$BSF = \frac{D}{d} \times \frac{N_r}{60} \times \left[1 + \left(\frac{d}{D} \right)^2 COS^2\beta \right] \text{ Hz} \quad (13)$$

Cage frequency

$$FTF = \frac{1}{2} \times \frac{N_r}{60} \times \left[1 - \left(\frac{d}{D} \right) COS\beta \right] \text{ Hz} \quad (14)$$

Varying compliance frequency (VC) = FTF · N_b Hz (15)

Where N_r, d, $'D$, N_b, β are rotational speed, roller diameter, pitch diameter, number of rolling elements and contact angle of the rolling element bearing, respectively. Analysis of frequencies and their corresponding amplitudes is an efficient method to detect bearing faults.

A bearing failure analysis considers faults developed on bearing contact surfaces, either by overloading the bearing or simulated faults on the roller bearing components. Artificial faults simulated on bearing components are not realistic; hence, there is a need to establish a correlation between naturally occurred surface fatigue wear and lubrication mechanisms in the normal operating conditions closer to the actual working conditions in various industrial applications. In this paper, wear propagation on the roller bearing component surfaces was assessed using specific film thickness analysis in conjunction with correction factors, wear mechanism analysis developed

on contact surfaces. Further, wear severity observed on the roller contact surfaces was justified using oil degradation and vibration signal analysis.

Experimental setup, sensors, equipment and data acquisition procedure

The primary objective of the experiment was to investigate wear propagation on bearing component surfaces under normal operating conditions. Lubricant temperature, lubricant film thickness, vibration signals and failure mechanisms were considered to assess operating conditions of the roller bearing. Figure 4 depicts the photograph of the experimental setup. The arrangement consists of a rotating mild steel shaft on which three bearings i.e.test bearing, load-bearing and support bearing, are mounted. The test bearing, which is an oil bath lubricated, is mounted on the right-hand side of the shaft while another end of the shaft consists of a ball bearing, which is coupled to the AC motor using jaw coupling. A load of 2.1 kN has been applied to the ball bearing, which is mounted on the housing at some distance offset to the test bearing, as shown in Figure 4. AC motor is controlled by using variable frequency drive, the speed of shaft was maintained at 600 rpm during the test and SAE 40 oil was used for the lubrication purpose. The inner race of the test bearing is fitted to the shaft using a steel bush; the test bearing is mounted in the bearing housing.

Figure 5 represents a block diagram of the experimental setup, a DEWE-43-DSA, 8-channel data acquisition system used to acquire vibration data at a regular time interval of 100 hours. Uniaxial accelerometer (MMF KS7800) was used to measure the vibration signals from the test bearing; the accelerometer is mounted on the central axis of bearing housing. The sensitivity of the accelerometer was 10.28 mV/m/s^2; each time domain was obtained after averaging ten sets of data, which seemed to be made residual noise negligible**.** The fatigue test experiments were conducted 8 hours in a day. A K-type thermocouple is used to measure the lubricant temperature; the

temperature is recorded continuously. After every 200 hours of operation, the bearing was dismounted and cleaned; the surface roughness values of the rolling components were measured by using a roughness tester. The wear developed on the inner race and roller surfaces was observed by using a USB microscope. The test bearing used in this experiment is SKF NJ307ECP; dimensions and specification of the bearing are shown in Table 1.

Measurement of lubricant rheology

Rheological analysis of lubricant is used to assess the degradation of lubricating oil. The rheological measurement was performed in the present work by using the Anton Paar rheometer (Physica MCR 301). All the analyses were carried out under control experimental conditions. The temperature of the rheometer plates was maintained at 25 °C, shear rate in the range of 0 to 1500 s^{-1} and heat generated between the plates was removed continuously, viscosity and shear rate values were recorded in the personal computer. The entire test was performed twice by repeating the same procedure.

Vibration Data acquisition procedure

The vibration signals were acquired using an MMFKS78100 uniaxial accelerometer. The accelerometer was mounted on the central axis of the housing in which the test bearing is mounted. Commercial data acquisition system Dew Soft 7.1 was used to acquire and store vibration data on a personal computer. The bearing vibration signals were acquired at a regular interval with a sampling frequency of 20 kHz.

Results and discussions

Specific film thickness analysis in conjunction with correction factors

A roller bearing's performance depends upon the formation of a separating fluid film between two rolling contact elements; therefore, estimation/measurement of fluid film thickness is essential to

assess the performance of a roller bearing. The lubricant temperature was measured from the inner race and roller contact zone; the corresponding viscosity of the lubricant was estimated by using a standard ASME temperature – viscosity chart. Figure 6 shows an increase in oil temperature as a function of operating time.

The prolonged operation increase in fatigue load cycles on the bearing components led to higher oil temperature and decreased stabilization time. In the present experiment, it was observed that for the fresh lubricating oil, stabilization temperature was found after 6 hours, whereas the stabilization temperature duration was reduced to 3 hours due to the degradation of oil. Hence, the overall temperature values of lubricant oil were increased during operation, as shown in Figure 6. The decrease in the stabilization time for lubricating oil is due to the heat generation and dissipation in the bearing system [13]. The corrected minimum film thickness and specific film thickness values were estimated using equation (5) and (6), respectively; these values are the indicators of lubrication regimes in the roller bearing. Figure 7 depicts a reduction in the minimum film thickness with respect to operating time in the location between bearing components, i.e., inner race and roller, outer race and roller are considered to estimate film thickness. The value of film thickness is higher at the outer race than the inner race; hence, the film thickness between the roller and inner race is critical, which is used to assess the bearing performance. The minimum film thickness as a function of operating time is shown in Figure 8; an increase in lubricant temperature led to a decrease in viscosity of the lubricant, which results in a significant reduction in the film thickness values.

The value of lubricant film thickness 1.2 µm, has been reduced to 0.92 µm after 1200 hours of operation. Further, prolonged operation causes wear propagation on rolling contact surfaces, which results in a subsequent degradation of lubricant oil. Hence, the film thickness values showed a

gradual decrease in trend with respect to an increase in fatigue load cycles, as shown in Figure 8. However, the actual operating condition of the lubricated machine elements revealed by specific film thickness analysis. Figure 9 (a) and (b) show the variation in specific film thickness (λ) with respect to the operating time. The fatigue test experiments were conducted over a period of 3000 hours. The transition in the lubrication regime is clearly highlighted in the diagrams. On the other hand, correction factors were also considered throughout the analysis to obtain reliable diagnostic information.

At the initial stage of operation, the specific film thickness value was eight; however, by considering the thermal and starvation correction factors, the specific film thickness value was reduced to 6.93, which confirms full film elastohydrodynamic lubrication regime in the bearing system. The specific film thickness values obtained until 700 hours were greater than 3, confirming the elastohydrodynamic regime. Further, after 700 hours, the specific film thickness values reduce to less than three, which results in the transition of the lubrication regime from elastohydrodynamic to the mixed lubrication regime in the bearing system. Bearing continues to operate in this regime up to 2200 hours; a continuous reduction in the specific film thickness values are observed in Figs. 9 (a) and (b). At the start of the mixed lubrication regime, a steady increase in wear severity was observed on the bearing components. At the end of the mixed lubrication regime, an increase in lubricant temperature and wear severity on the rolling contact surfaces causes an increase in the combined surface roughness of rollers and inner race, which ultimately results in a reduction in the specific film thickness, thereby causing a transition of lubrication regime from mixed lubrication regime to BL regime. Estimating specific film thickness in conjunction with correction factors, provides reliable information about transition in lubrication regimes, as shown in Figure 10. Actual film thickness values play an important role in the wear

assessment of a bearing system. There is direct metal-to-metal contact in the boundary lubrication regime, and lack of lubricating action between the inner race and roller causes an increase in lubricant temperature and wear propagation on rolling contact surfaces.

Lubricating oil rheology

The rheological behavior of degraded lubricating oil is measured by using flow curves obtained at 25 ^{0}C. Figure 11 (a) - (c) depict the flow curves of lubricating oil at EHL, mixed lubrication and BL regimes. It is observed that dynamic viscosity decreases sharply with an increase in shear rate, which shows the non-Newtonian behavior of lubricant. The dynamic viscosity of the fresh oil decreases from 0.297 N. s/m^2 to 0.275 N. s/m^2. This decrease in dynamic viscosity is due to viscous heating and temporary alignment of the lubricating oil molecules. Further, the flow curve of lubricant samples collected after 500, 1000, 1500, 2000, 2500, 3000 hours of operation show the decrease in dynamic viscosity for both the low and high shear rates, as shown in Figure 11(a) – (c). The lubricant used in the bearing under the EHL contact is subjected to the higher stresses and velocities between the two races. Under such operating conditions, permanent stretching of the lubricant molecules occurs, causing a gradual decrease in viscosity value in aged lubricant samples. At the high shear rate, the degraded lubricant showed a reduction in the dynamic viscosity values from 0.297 N. s/m^2 at fresh oil to 0.195 N. s/m^2 at the end of the test. The decreasing trend in the dynamic viscosity due to mechanical degradation continues with an increase in the operating time. The degraded lubricant sample collected after 3000 hours showed the dynamic viscosity values of 0.195 N. s/m^2 and 0.169 N. s/m^2 for low and high shear rates. This decrease in the dynamic viscosity of lubricant due to an increase in fatigue load cycles and mechanical degradation affects the operating performance of the machine elements.

Microscopic observation of surface fatigue wear

To correlate the effects of a reduction in specific film thickness and oil degradation to the change in the dynamic response of the bearing system, the physical observation of wear propagation at various lubrication regimes has been considered. Figure 12 (a) and (b) represent the optical micrographs of different sections of the inner race observed during the EHL regime. Figure 12 (a) represents smooth rolling surfaces obtained after the run-in wear test after 100 hours. The rolling contact surfaces are separated by a thick lubrication film in the elastohydrodynamic lubrication regime, which resulted in a micro pitting on the inner race, as shown in Figure 12 (a).

With the increase in operating cycles, the micro-pitting on the rolling element bearing continues to propagate. Figure 12 (b) shows the inner race surface observed after 800 hours, an increase in micro pitting wear on the contact surfaces of bearing led to an increase in surface roughness. As a result, a lubrication regime transition takes place from elastohydrodynamic lubrication to a mixed lubrication regime. Figure 12 (c) and (d) indicate an increase in the distribution of micro-pits, surface cracks on the inner race surface in the mixed lubrication regime. Due to lubricant degradation and an increase in surface fatigue wear on the rolling surfaces, the effective specific film thickness between the two races continues to decrease, leading to increased direct metal-to-metal contact between two rolling elements. After 2200 hours, the lubrication regime of the bearing transits from the mixed lubrication regime to the boundary lubrication regime. Figure 12 (d) shows the inner race surface on which macro pits and spalling defects are present. Scuffing is also appeared on the inner race due to a reduction in the specific lubricant film thickness. Further, prolonged operation of bearing in boundary lubrication regime during 2200 hours to 3000 hours triggers severe wear on the inner race, roller and outer race surfaces of bearing; these defects are depicted in Figure 12 (e) and (f).

USB optical microscopic provides a surface examination in two-dimension under low resolution; however, to obtain a better resolution and detailed analysis of wear defects in three-dimensions, the confocal laser scanning microscope (CLSM) was used. Confocal laser scanning microscopy is a promising technique for wear characterization with 2D and 3D surface topographies. On the other hand, CLSM provides surface texture properties, i.e., surface roughness and waviness parameters. In the present work, CLSM was used to obtain a three-dimensional image of rolling bearing surfaces; three-dimensional images obtained under EHL, Mixed lubrication and BL regimes are shown in Figure 13 (a)-(e). Three-dimensional micrographs obtained in the EHL regime are presented in Figure 13 (a) and (b), which depict micro pits and mild wear on rolling surfaces in the EHL regime. The areal field parameter average roughness (S_a) measured over the three-dimension surface is 0.343 µm. The surface condition of the inner race observed in the mixed lubrication regime after 1500 hours is shown in Figure 13 (c) and (d); an increase in the depth and width of pit size is observed in the CLSM micrographs. The value of the average areal surface roughness in the mixed lubrication regime was 0.484 µm. The worn inner race surfaces found in the boundary lubrication regime are represented in Figure 13 (e) and (f). A large spall spread over the inner race surface is depicted in Figure (e), which appeared due to excessive contact fatigue wear. Figure 13 (f) indicates the deep and large scoring damage developed due to abrasive wear on inner race surfaces, the increase in (S_a) value 3.72 µm shows the severity of the wear.

Effect of transition in the lubrication regimes on vibration signals

The statistical features of the vibration signals are represented in Figure 14 (a) - (d). The RMS values of the vibration signals showed an increasing trend, with an increase in the operating time, as shown in Figure 14 (a). The RMS value obtained from the newly installed bearing was 3.48 m/s^2; after running in wear period of 100 hours, the RMS value decreased to 3.07 m/s^2; a small decrement

was observed in the RMS value. After 700 hours of operation, there is a moderate increment in the RMS values due to surface fatigue wear. In the mixed lubrication regime, the RMS values increased from 3.8 m/s^2 to 8.2 m/s^2 during 700-2200 hours of operation. When the bearing enters the boundary lubrication regime, the RMS value increased from 8.2 m/s^2 to 13.5 m/s^2 in just 500 hours, indicating severe and rapid degradation of the bearing surfaces.

Figure 14 (b) shows the crest factor values of vibration signals with respect to operating time. At the initial stage of the experiment, the crest factor value was found to be 2.4; a steady increase in trend is observed in the elastohydrodynamic and mixed lubrication regime. In the boundary lubrication regime, after 2200 hours, the crest factor values showed a steep increase in trend due to an increase in the size faults developed on the bearing components.

Figure 14 (c) shows a plot of kurtosis values versus operating time; at the initial stage of the fatigue test, the kurtosis value of the vibration signal was around 2.7. Further, an increase in the localized defects such as pitting, scuffing, scoring and spalling results increases the strength of bearing vibration signals, leading to a rise in kurtosis values. In the elastohydrodynamic regime, the kurtosis values are around 2.8 - 3, which indicates a healthy state of the bearing. When bearing the lubrication regime transits from EHL to the mixed regime, there is no significant change in the kurtosis value. A considerable variation in the kurtosis values was observed after 1000 hours; the development of localized defects on the rolling surfaces results in a drastic increase in kurtosis values up to 5.0. Further, after 2200 hours, when the lubrication regime reaches the boundary lubrication, an abnormal increase in the kurtosis values is very similar to the RMS and crest factor values. The kurtosis values in the boundary lubrication regime increased from 5 to 6.2, indicating wear severity on the bearing surfaces. On the other hand, an increasing trend on the peak-to-peak

values of vibration signals depicted in Figure 14 (d) also shows a similar pattern observed in the aforementioned statistical parameters.

The correlation between operating time, on transition in lubrication regimes and vibration response of the bearing system, is depicted using 3-D surface plots. Figure 15(a) – (c) shows a variation in the vibration response of the bearing system obtained in EHL, Mixed lubrication and BL regimes. At the initial stage of operation, the elastohydrodynamic lubrication system exits in the bearing system up to 700 hours. This lubrication regime results in mild wear on the bearing contact surfaces and lower vibration levels, as shown in Figure 15 (a). As the lubrication regime transition, i.e., EHL to mixed lubrication, took place after 700 hours, mixed lubrication regime exists over the longer duration from 700 hours to 2200 hours. A steady increase in RMS values has been observed in the mixed lubrication regime up to 1800 hours.

Further, a drastic increase in RMS values occurs due to severe surface fatigue wear propagation on the rolling contact surfaces, the variation in the RMS and λ values as a function of operating time in the EHL regime is shown in Figure 15 (b). An increase in fatigue load cycles led to surface fatigue wear, which resulted in higher surface roughness values. The surface roughness is a crucial parameter, which causes a transition in the lubrication regime. After 2200 hours, a change took place from mixed lubrication to BL regime, thereby resulting in a significant increase in RMS values, as shown in Figure 15 (c); 3-d Plots show the dependency of vibration data on specific film thickness values and increase in operating time.

Bearing vibration spectrum analysis

A statistical measurement of vibration signals provides useful information on the overall evaluation of bearing defects; however, the statistical features do not provide accurate size and

exact location of the localized defects developed in the bearing components [7,8]. The spectrum analysis is extensively used to understand the characteristics of the vibration signals and to locate the defects in roller bearing components. The vibration spectra of the roller bearing acquired during the experiments are represented in Figure 16 (a-e); the frequency range considered in the spectrum plot is 0 to 300 Hz. The vibration spectrum obtained after 200 hours under the elastohydrodynamic lubrication regime is shown in Figure 16 (a); the peaks appeared in the spectrum are related to the rotational frequencies of bearing components and their higher multiples.

Figure 16 (b) depicts the vibration response obtained after 700 hours, at the end of the EHL regime. A rise in inner race malfunction frequency amplitude is observed in the vibration spectrum along with peak related to multiple bearing compliance frequencies. From this Figure, it can be concluded that faults have been developed on the inner race surfaces. The microscopic images are shown in Figure 12 (b) highlight micro-pitting, scratch marks along with small size pits on the inner race at the initial stage of the mixed lubrication regime. The vibration spectrum obtained after 1500 hours is depicted in Figure 16 (c); the dominant amplitudes of frequency in this spectrum is observed at the inner race characteristic frequency and its multiple harmonics 1fi, 2 fi and 3 fi along with the interaction effect of shaft rotational frequencies,

which are highlighted as $1f_i$-X, $2f_i$-X, and 4VC in the spectrum. After 2200 hours of continuous operation, the transition occurs from the mixed lubrication regime to the boundary lubrication regime. This change caused an increase in the trend of statistical parameters, as shown in Figure 14. Similarly, a noticeable difference can be observed in the frequency spectrum.

The boundary lubrication regime results in various wear mechanisms on the rolling contact surfaces of the bearing along with metal-to-metal contact. Figure 16 (d) represents the vibration

spectrum of the roller bearing obtained after 2400 hours. In the vibration spectrum, increase in vibration amplitudes appeared at roller, inner race characteristic frequencies 1 *fr*, 1*fi*, 2*fi* and 3*fi* which indicate surface fatigue wear propagation on rollers and inner race contact surfaces. The boundary lubrication regime results in the fast development of surface fatigue wear on all the bearing component surfaces. Figure 16 (e) depicts the vibration spectrum obtained after 3000 hours; higher amplitude peaks, which correspond to inner race, outer race and ball defects along with their multiple harmonics have appeared in the spectrum due to the severe defects developed in the bearing components under boundary lubrication regime.

Summary and conclusions

In this work, the development of surface fatigue wear on the contact surfaces of roller bearing has been investigated by considering specific film thickness analysis in conjunction with correction factors. Transition in lubrication regimes results in lubricant oil degradation, development of surface fatigue faults, thereby causing abnormal vibrations in the bearing system. The following conclusions were drawn from the experimental observations.

(1) The specific film thickness was estimated and correlated with wear propagation on the roller bearing surfaces in conjunction with Stribeck curve analysis. The reduction in lubricant film thickness between the rolling contact results in various surface fatigue wear defects on the bearing components.

(2) The transition in lubrication regimes and oil degradation analysis were correlated with wear and statistical parameters of vibration signals acquired from the bearing system.

(3) The microscopic observations showed that at the initial stage, wear appeared on the inner race, a further increase in fatigue load cycles result in the development of wear on the roller and outer race surfaces.

(4) Rheological studies of lubricating oil showed a considerable reduction in lubricant viscosity as a result of oil degradation.

Wear reduction on bearing components is also equally important in bearing design; enhancement in lubricant properties plays a significant role in minimizing wear in lubricated machine components. Nanoparticle additives are gaining their importance in improving the physical, chemical and rheological properties of lubricants. The enhancement in lubricant properties reduces wear in lubricated machine elements subjected to fatigue load cycles. Efforts are being made to utilize multi-wall carbon nanotubes (MWCNTS) applications to minimize wear in rolling element bearings; authors expect a significant reduction of wear, vibration, and noise levels in the bearing system subjected to the same operating conditions presented in this work.

Nomenclatures:

$C_{starvation}$	starvation correction factor
$C_{thermal}$	thermal correction factor
D_i	inner bore diameter (mm)
D_o	outside ring diameter (mm)
d_i	roller diameter (mm)
d_m	pitch diameter (mm)
E'	equivalent modulus of elasticity, N/m^2

E'	$\frac{2E_1E_2}{E_2\left(1-\sigma_1^2\right)+E_1(1-\sigma_2^2)}$
E_1, E_2	modulus of elasticity of inner race and roller material respectively, N/m^2
F	load (N)
G	dimensionless material parameter
h	fully flooded film thickness, µm
h^*_{min}	corrected film thickness, µm
h_{min}	minimum film thickness, µm
h_e	length of the film thickness
k	thermal conductivity of lubricant, w/m-K
L	length of rollers, mm
N	number of rollers
P_H	maximum Hertzian pressure (MPa)
R_x	effective radii of curvature, mm
R_X	$\left(\frac{1}{R_1}+\frac{1}{R_2}\right)$
R_1, R_2	radius of curvature of inner race and roller, mm
R^2_{q1}	RMS value of surface roughness of roller
R^2_{q2}	RMS value of surface roughness of inner race
Ra	average roughness
S	slide to roll ratio
U_r	dimensionless speed parameter
u	average rolling velocity, m/s
W	dimensionless load
W_{max}	load applied, N

μ_0	absolute viscosity, N-s/m^2
α	pressure viscosity coefficient, m^2/ N
λ	specific film thickness
σ_1, σ_2	Poisson's ratio of the inner race and roller material respectively
η_0	inlet viscosity of the lubricant, Pa-s
γ	temperature-viscosity coefficient of lubricant, 1/K
φ_s	starvation factor
β	contact angle

References

1. Zhang, J., Drinkwater, B.W., Dwyer-Joyce, R.S.: Monitoring of Lubricant Film Failure in a Ball Bearing Using Ultrasound. J Tribol. **128 (3**), 612-618 (2006).
2. Jena, D.P., Panigrahi, S.N.: Precise measurement of defect width in tapered roller bearing using vibration signal. Meas J Int Meas Confed. **55**, 39–50 (2014).
3. Ben Ali, J., Fnaiech, N., Saidi, L., Chebel-Morello, B., Fnaiech, F.: Application of empirical mode decomposition and artificial neural network for automatic bearing fault diagnosis based on vibration signals. Appl Acoust. **89**, 16–27 (2015).
4. Kankar, P.K., Harsha, S.P., Kumar, P., Sharma, S.C.: Fault diagnosis of a rotor bearing system using response surface method. Eur J Mech A/Solids **28**, 841–57 (2009).
5. Mathew, J., Alfredson, R.J.: The Condition Monitoring of Rolling Element Bearings Using Vibration Analysis. J Vib Acoust. **106**, 447–53 (1984).
6. Amarnath, M., Lee, S.K.: Assessment of surface contact fatigue failure in a spur geared

system based on the tribological and vibration parameter analysis. Meas J Int Meas Confed. **76**, 32–44 (2015).

7. Yusof, N.F.M. and Ripin, Z.M.: Analysis of Surface Parameters and Vibration of Roller Bearing Analysis of Surface Parameters and Vibration of Roller Bearing. Tribol Trans. **57(4**), 37–41 (2014).

8. Karacay, T., Akturk, N.: Experimental diagnostics of ball bearings using statistical and spectral methods. Tribol Int. **42**, 836–43 (2009).

9. Ueda, T., Mitamura, N.: Mechanism of dent initiated flaking and bearing life enhancement technology under contaminated lubrication condition. Part II: Effect of rolling element surface roughness on flaking resulting from dents, and life enhancement technology of rolling bearings. Tribol Int. **42**, 1832–37 (2009).

10. Al-Ghamd, A.M., Mba, D. A comparative experimental study on the use of acoustic emission and vibration analysis for bearing defect identification and estimation of defect size. Mech Syst Signal Process **20**, 1537–71 (2006).

11. Koulocheris, D., Stathis, A., Costopoulos, T., Tsantiotis, D.: Experimental study of the impact of grease particle contaminants on wear and fatigue life of ball bearings. Eng Fail Anal. **39**, 164–80 (2014).

12. Zong, H., Hua, W., Tian, S., Gao, X.: A life test method and result analysis for slewing bearings in wind turbines. Proc Inst Mech Eng Part C J Mech Eng Sci. **229**, 3499–514 (2015).

13. Serrato, R., Maru, M.M., Padovese, L.R.: Effect of lubricant viscosity grade on mechanical vibration of roller bearings. Tribol Int. **40**, 1270–75 (2007).

14. Lee, S., Amarnath, M.: Experimental investigations to establish correlation between Stribeck curve , specific film thickness and statistical parameters of vibration and sound signals in a spur gear system. Jounral Vib Control **22(6)**, 1667-81 (2014).

15. Halme, J., Andersson, P.: Rolling contact fatigue and wear fundamentals for rolling bearing diagnostics - State of the art. Proc Inst Mech Eng Part J J Eng Tribol. **224,** 377–93 (2010).

16. Hamrock, B.J.: Fundamentals Fluid Film Lubrication McGraw-Hill (1991).

17. Zhang, Y., Liu, H., Zhu, C., Liu, M., Song, C.: Oil film stiffness and damping in an elastohydrodynamic lubrication. Journal of Mechanical Science and Technology **30**, 3031–39 (2016).

18. Hamel, M., Addali, A., Mba, D.: Investigation of the influence of oil film thickness on helical gear defect detection using Acoustic Emission. Appl Acoust. **79**:42–6 (2014).

19. Jang, J.Y., Khonsari, M.M.: Elastohydrodynamic line - contact of compressible shear thinning fluids with consideration of surface roughness. Journal of Tribol. **132(3)**, 034501-6 (2010).

20. Lugt, P.M.: A Review of Elasto-Hydrodynamic Lubrication Theory A Review of Elasto-Hydrodynamic Lubrication Theory. Tribology Trans. **54(3)**, 470-496 (2011).

21. Ebner, M., Yilmaz, M., Lohner, T., Michaelis, K., Höhn, B., Stahl, K.: On the effect of starved lubrication on elastohydrodynamic (EHL) line contacts. Tribol Int. **118**, 515-523 (2017)

22. Zhu, D., Wang, J., Ren, N., Wang, Q.J.: Mixed Elastohydrodynamic Lubrication in Finite Roller Contacts Involving Realistic Geometry and Surface Roughness. J Tribol. **134(1)**, 11504-14 (2012).

23. Jacobson, B.: Thin film lubrication of real surfaces. Tribol Int. **33**, 205–10 (2000).

24. Olver, A.V.: The mechanism of rolling contact fatigue: An update. Proc Inst Mech Eng Part J J Eng Tribol. **219**, 313–30 (2005).

25. Bormetti, E., Donzella, G., Mazzù, A.: Surface and Subsurface Cracks in Rolling Contact Fatigue of Hardened Components. Tribology Trans. **45(3)**, 274–283 (2002)

26. Dowson, D.: Elastohydrodynamic and micro-elastohydrodynamic lubrication. Wear, **190(2)**, 125–38 (1995).

27. Booser, E.R.: Handbook of Lubrication (Tribology) **vol. II** (1983).

28. Takabi, J., Khonsari, M.M.: On the dynamic performance of roller bearings operating under low rotational speeds with consideration of surface roughness. Tribology Int. **86,** 62–71(2015).

29. Kumar, P., Kumar, N.: Surface Roughness Effects in Pure Sliding EHL Line Contacts with Carreau-Type Shear-Thinning Lubricants; World Academy of Science, Engineering and Technology International Journal of Mechanical and Mechatronics Engineering **8(6)**, 1108–1113 (2014)

30. Hsu, C.H., Lee, R.T.: An Efficient Algorithm for Thermal Elastohydrodynamic Lubrication Under Rolling / Sliding Line Contacts. J Tribol. **116(4)**, 762-769 (1994).

31. Gupta, P.K.: Advanced Dynamics of Rolling Elements (1986).

32. Bair, S., Krupka, I., Sperka, P., Hartl, M.: Tribology International Quantitative elastohydrodynamic film thickness of mechanically degraded oil. Tribology Int. **64**, 33–8 (2013).

33. Santos, J.C.O., Santos. I.M.G., Souza, A.G.: Thermal degradation of synthetic lubricating oils : Rheological study Part II. Pet Sci Technol **35**, 535–9 (2017).

34. Santos, J.C.O., Santos, I.M.G., Souza, A.G., Sobrinhoc, E.V., Jr., S.J.F., Silva, A.J.N.: Thermoanalytical and rheological characterization of automotive mineral lubricants after thermal degradation. Fule, **83**, 2393–9 (2004).

35. Mansour, A.M., Al-maamari, R.S., Al-hashmi A.S., Zaitoun, A., Al-sharji, H.: Journal of Petroleum Science and Engineering In-situ rheology and mechanical degradation of EOR polyacrylamide solutions under moderate shear rates. J Pet Sci Eng. **115**, 57–65 (2014).

36. Sargent, L.B.: Pressure-Viscosity Coefficients of Liquid Lubricants. A S L E Transactions **26**, 37–41 (2008).

37. Sujatha, C.: Vibration and acoustics: measurement and signal analysis. Tata McGraw Hill Education Private Limited (2010).

38. Taylor, I.J.: Identification of Bearing Defects by Spectral Analysis. Journal of Mechanical Design, Transaction of ASME **120**, 199-204 (1980)

39. Shigley, J.E., Mishke, C.R.: Standard Handbook of Machine Design. 2nd ed., McGraw Hill (1996).

Figures

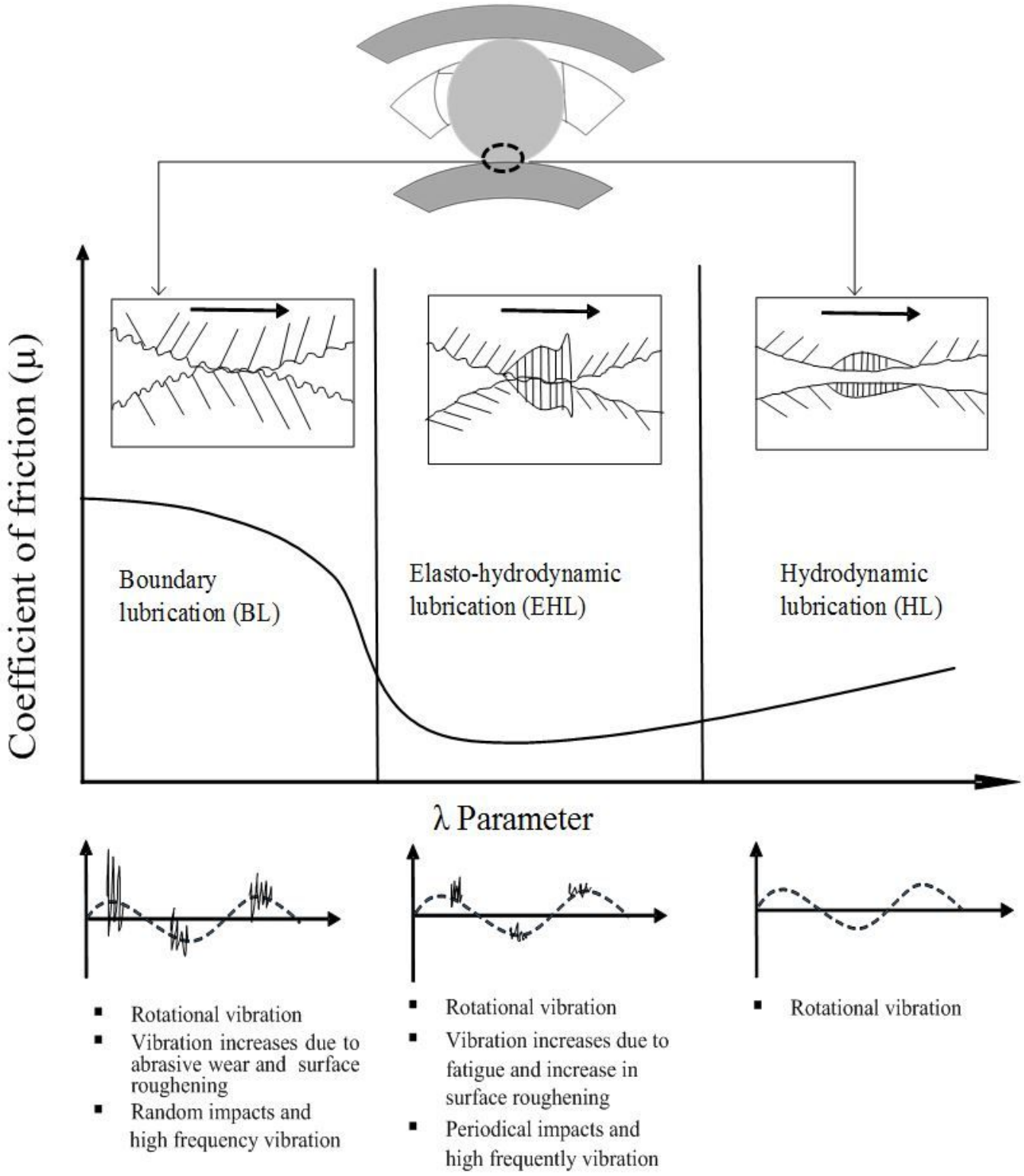

Figure 1

Transition of lubrication regime in roller bearing and corresponding effects on dynamic response [14,15]

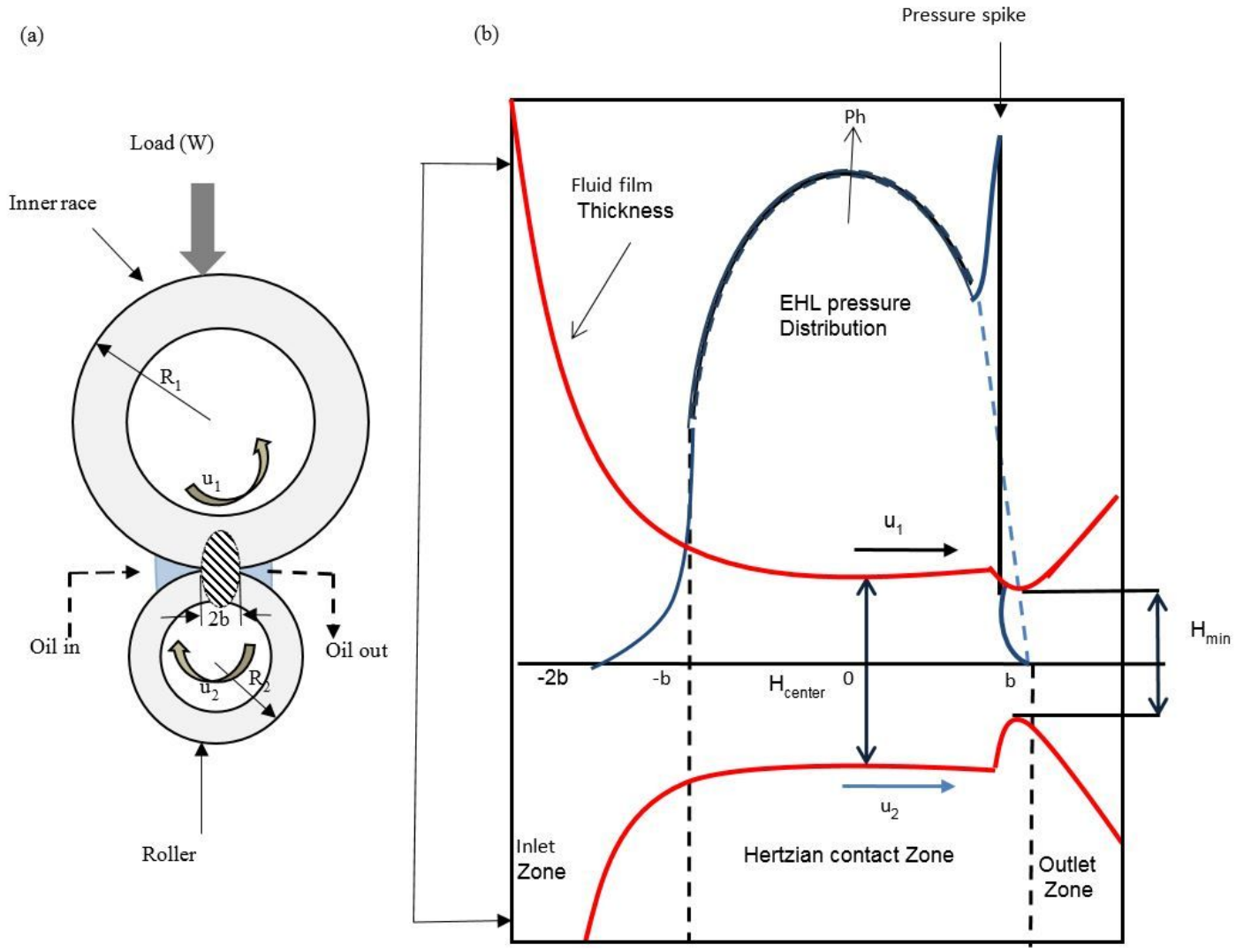

Figure 2

Film thickness formation in EHL contact (a) roller contact (b) enlarged view [21,22]

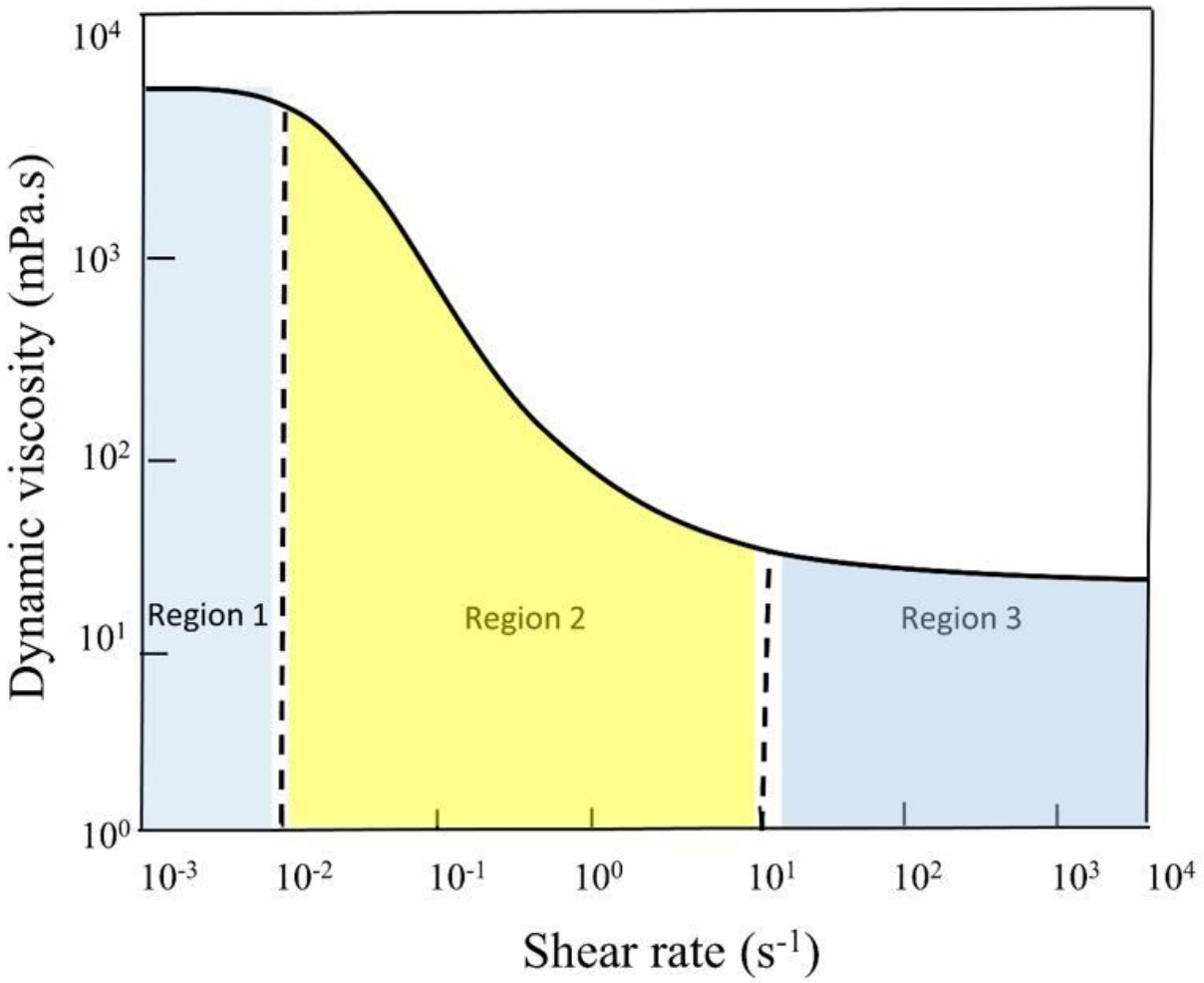

Figure 3

Schematic representation of the flow curve of lubricating oil

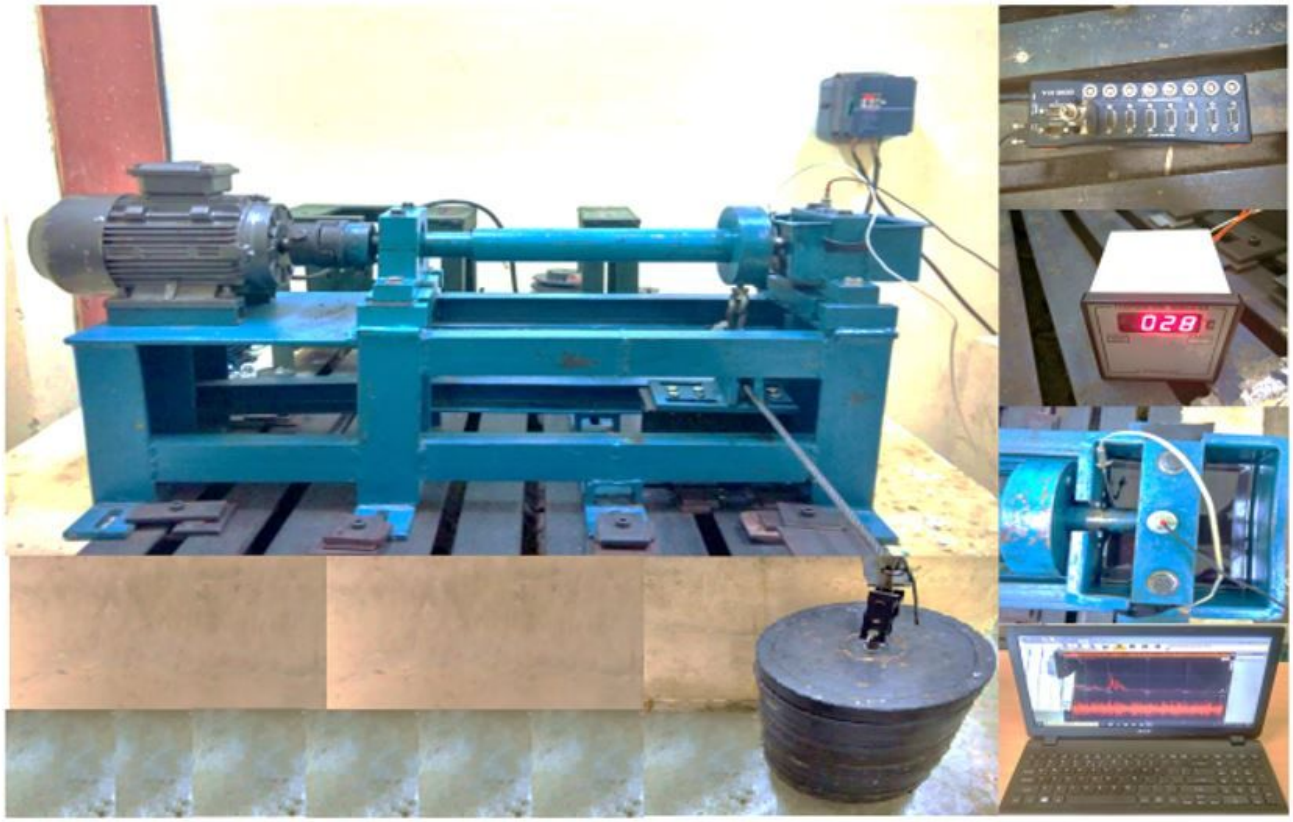

Figure 4

Photograph of the experimental test rig

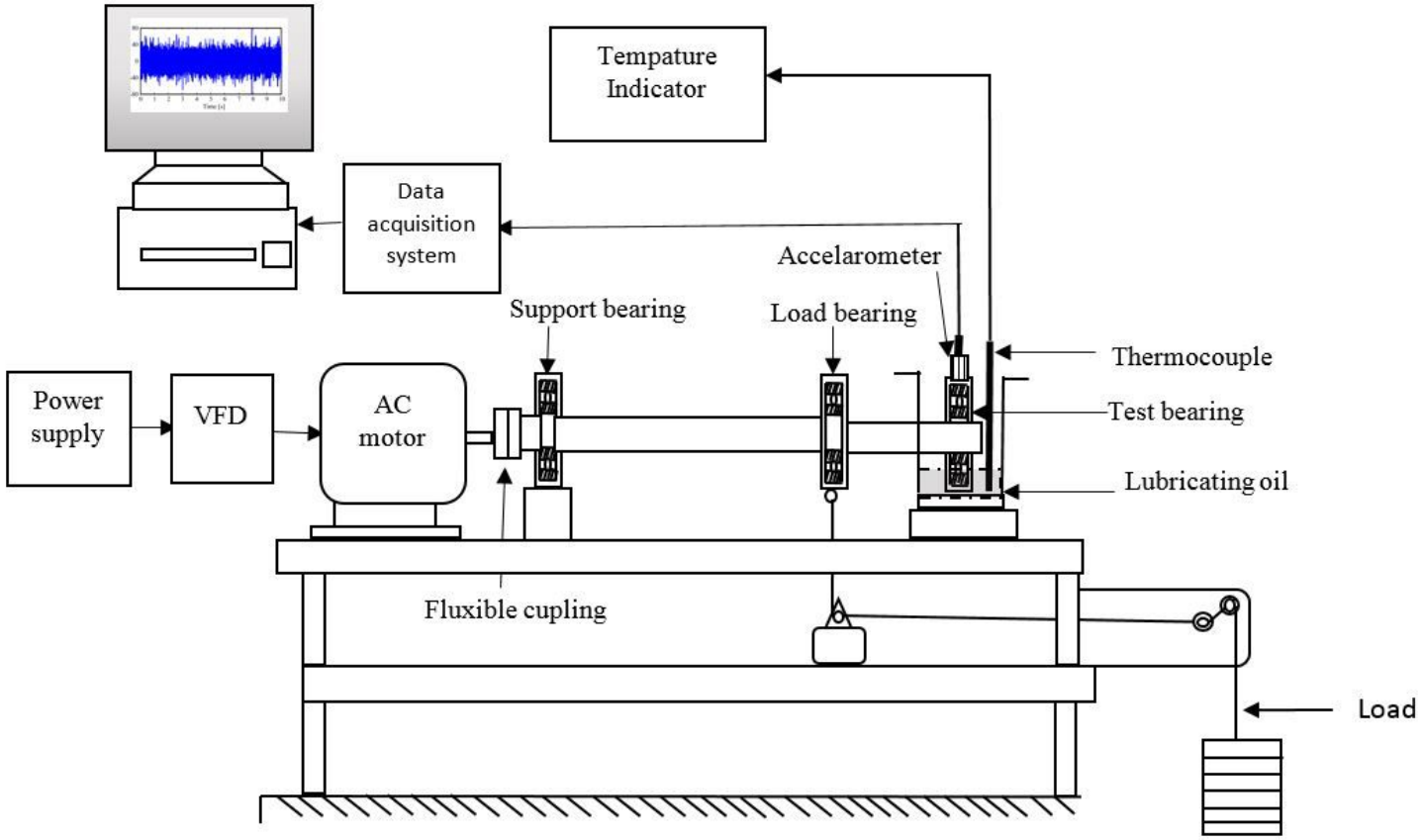

Figure 5

Schematic diagram of the experimental setup

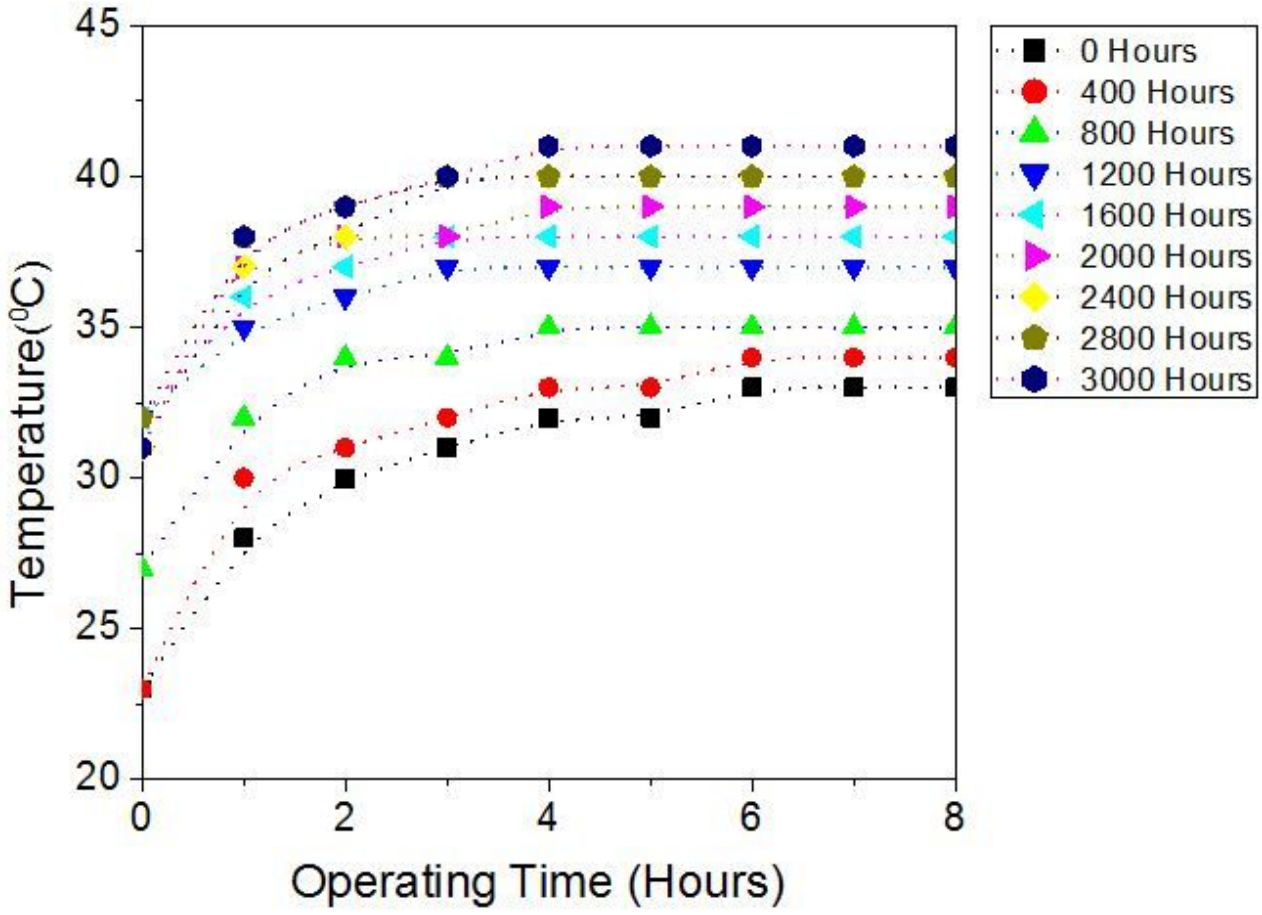

Figure 6

Lubricant oil temperature versus operating time

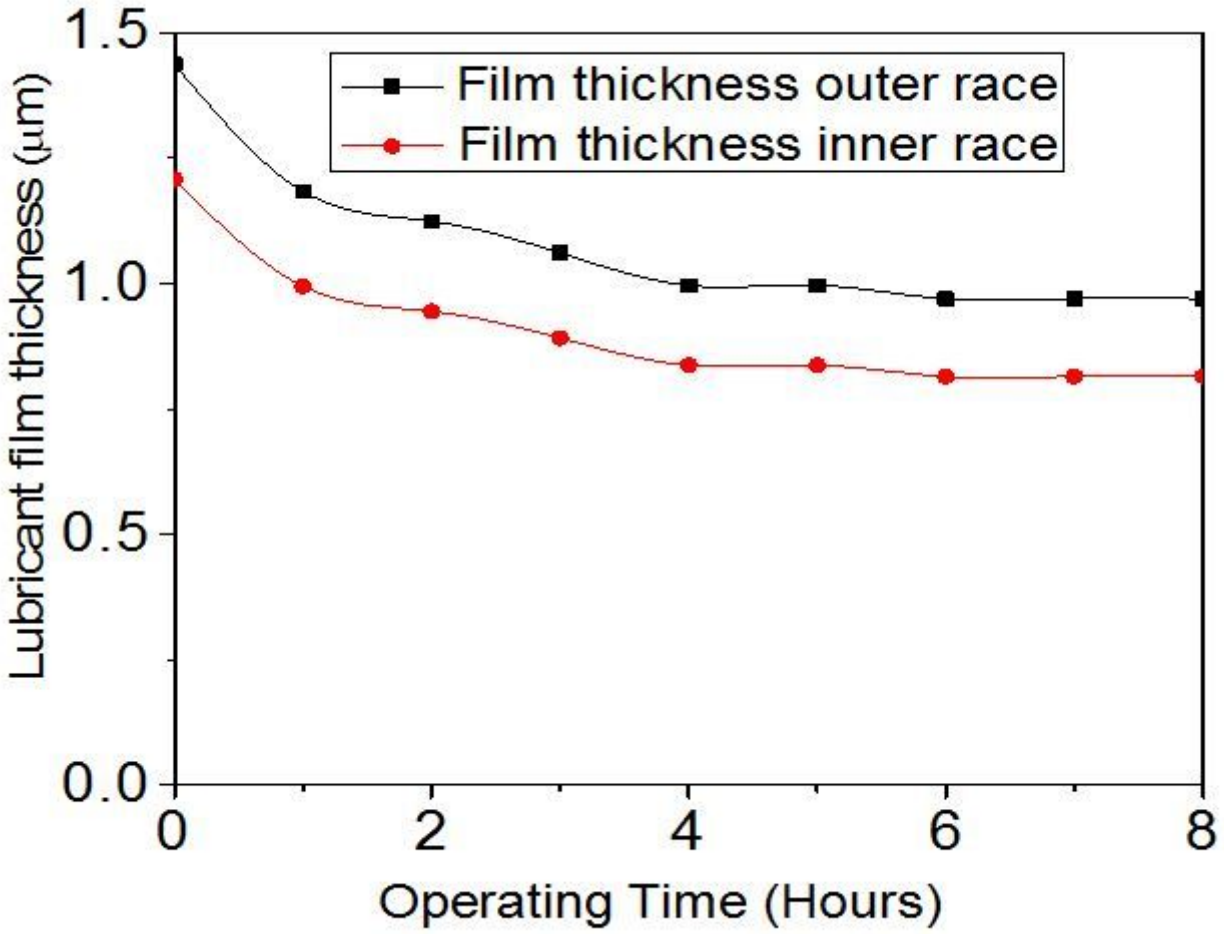

Figure 7

Lubricant film thickness versus operating time

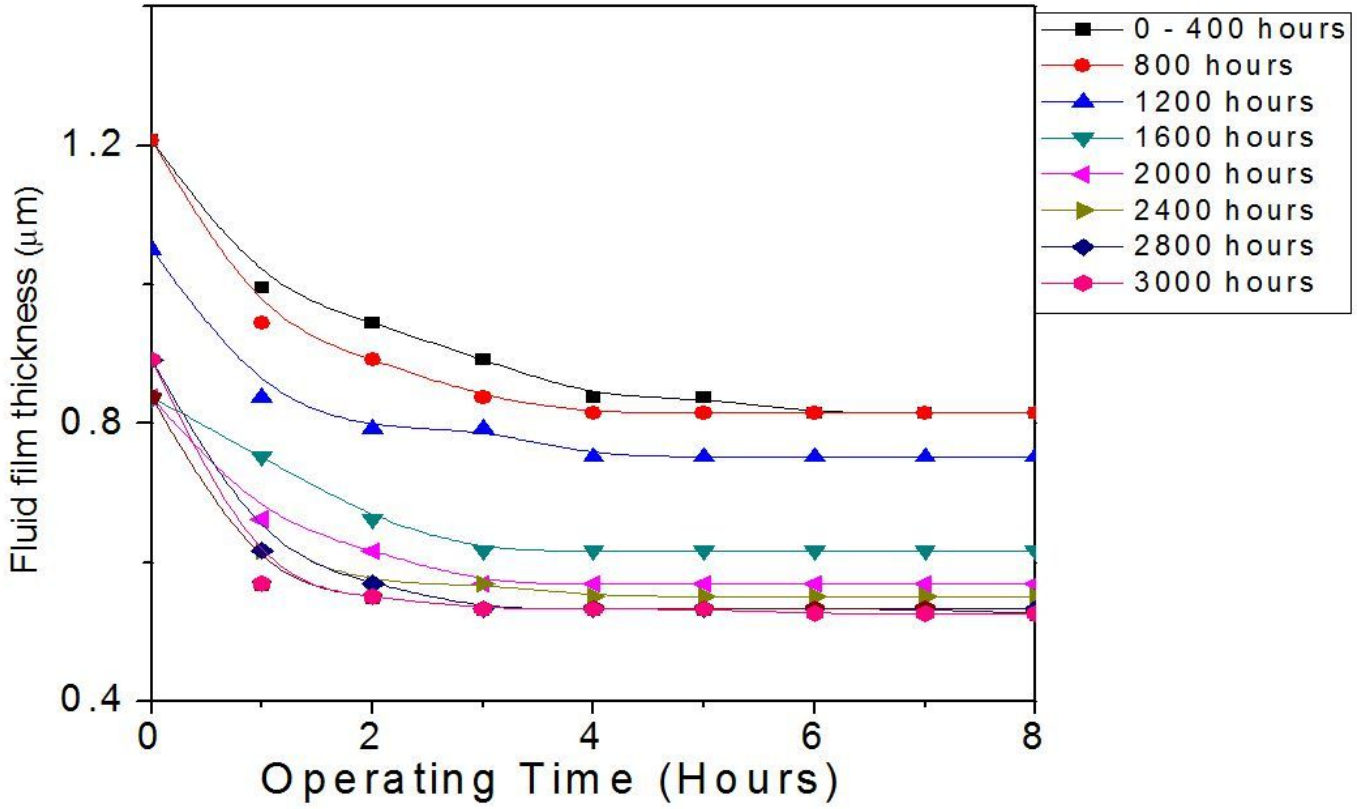

Figure 8

Lubricant film thickness vs. operating time throughout the experiment

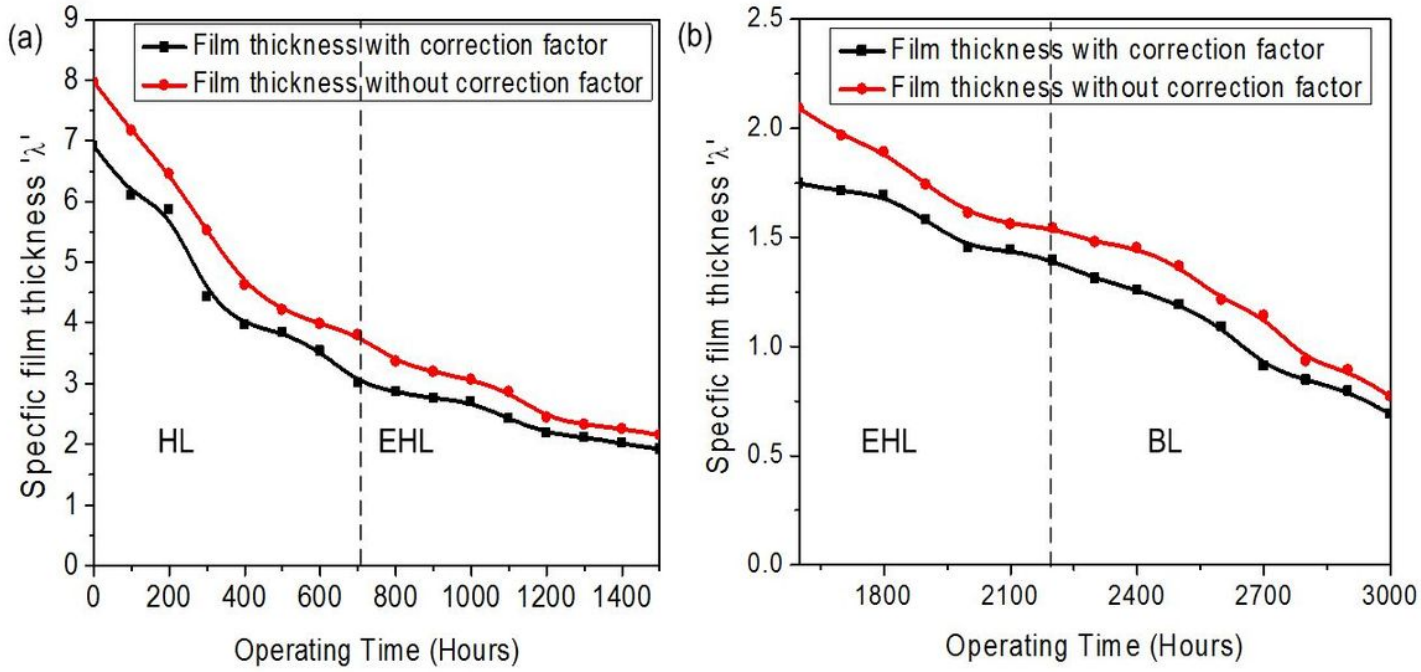

Figure 9

Observation on transition in lubrication regime (a) HL to EHL (B) EHL to BL

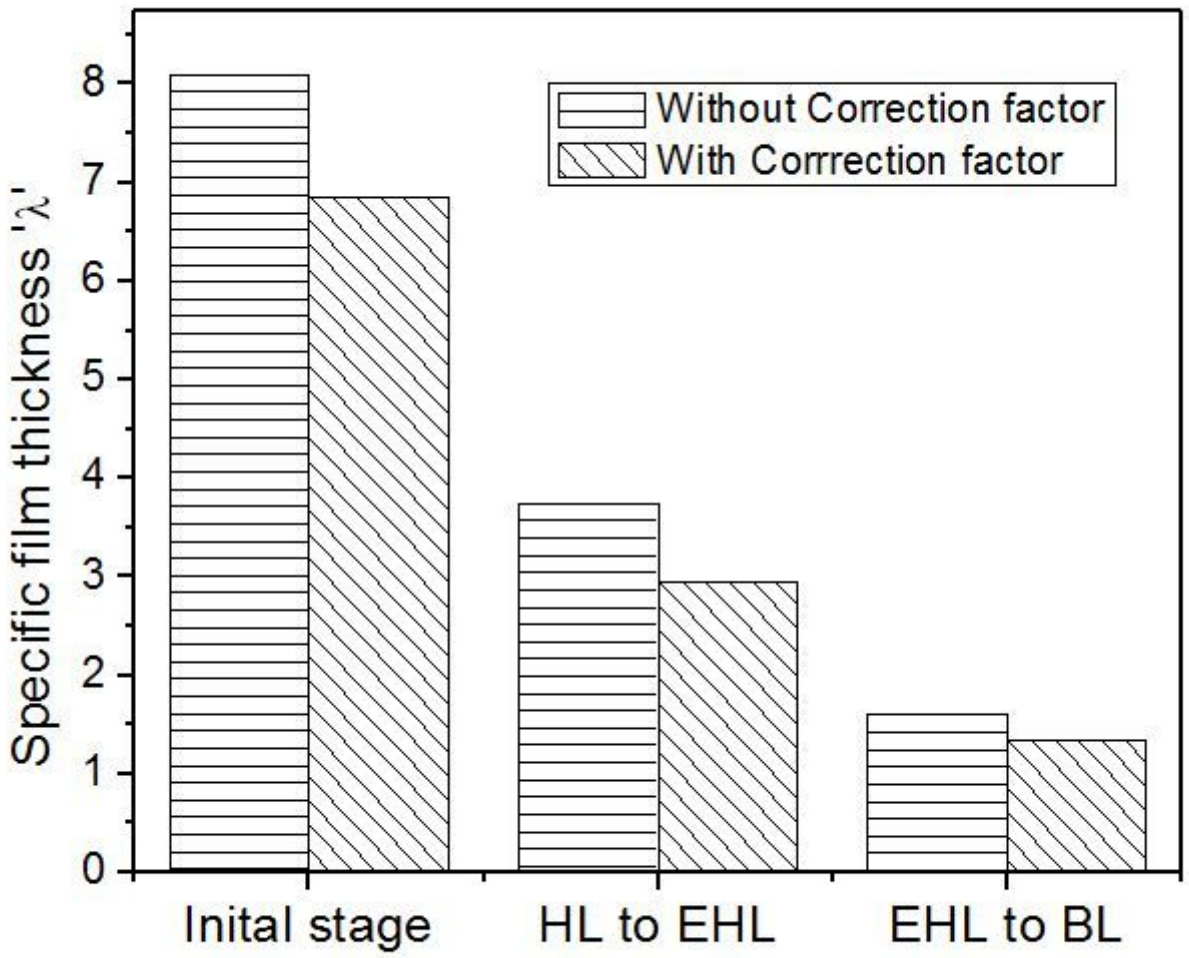

Figure 10

Importance of correction factor in lubrication regime analysis

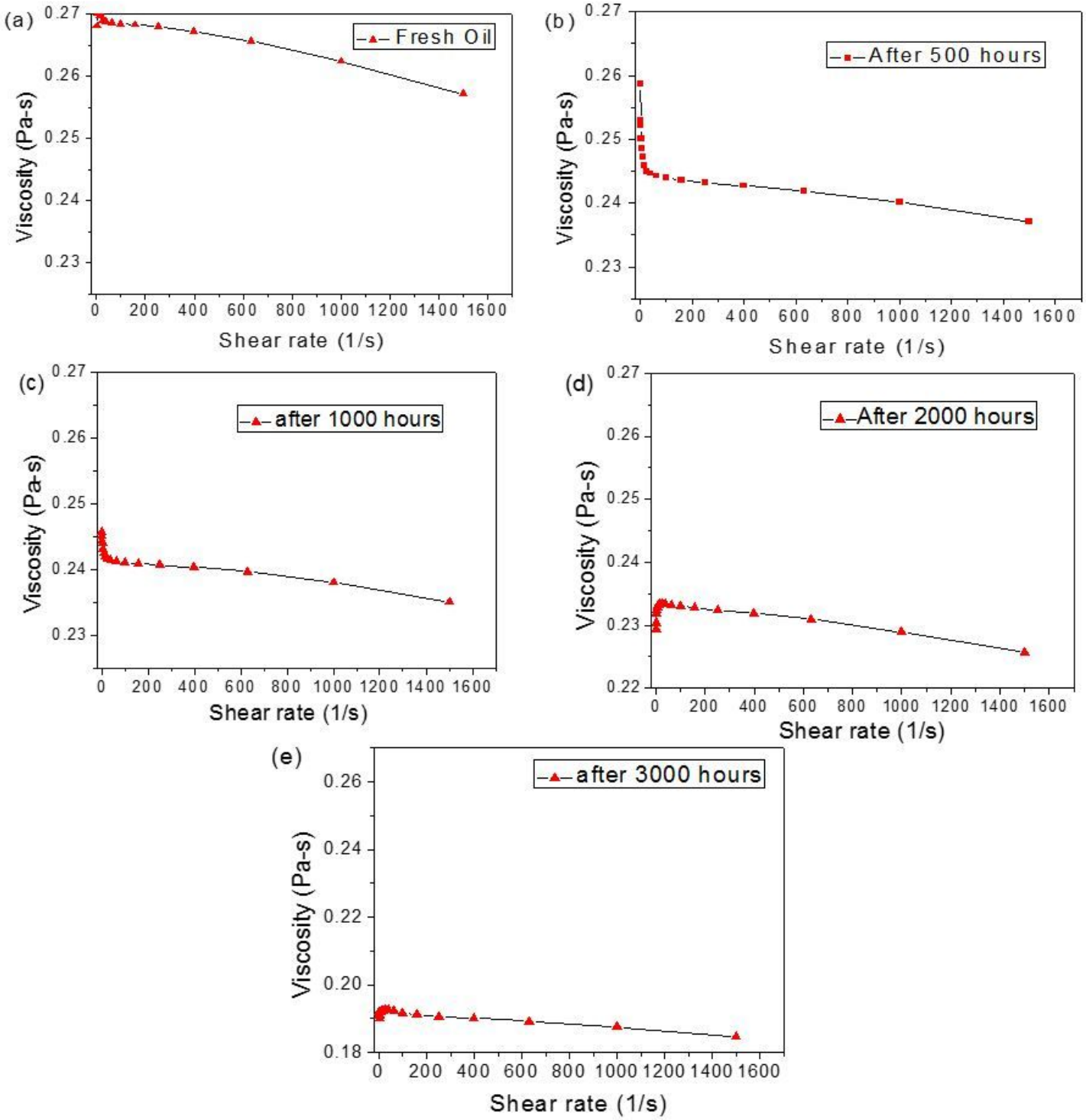

Figure 11

Dynamic viscosity vs. shear rate (a) new oil (b) after 500 hours (c) after 1000 hours (d) After 2000 hours (e) after 3000 hours

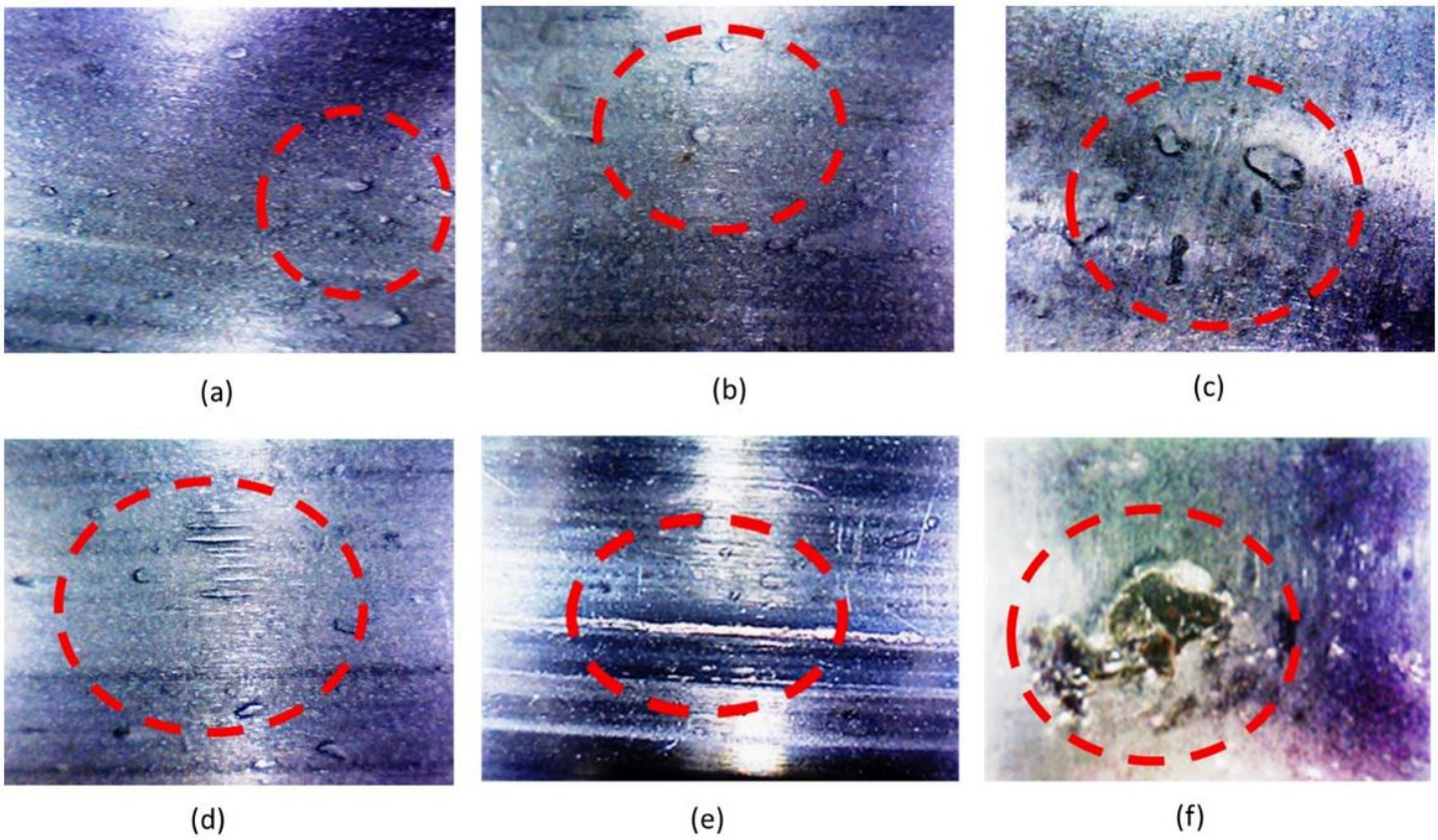

Figure 12

Visual inspection of wear on the inner race

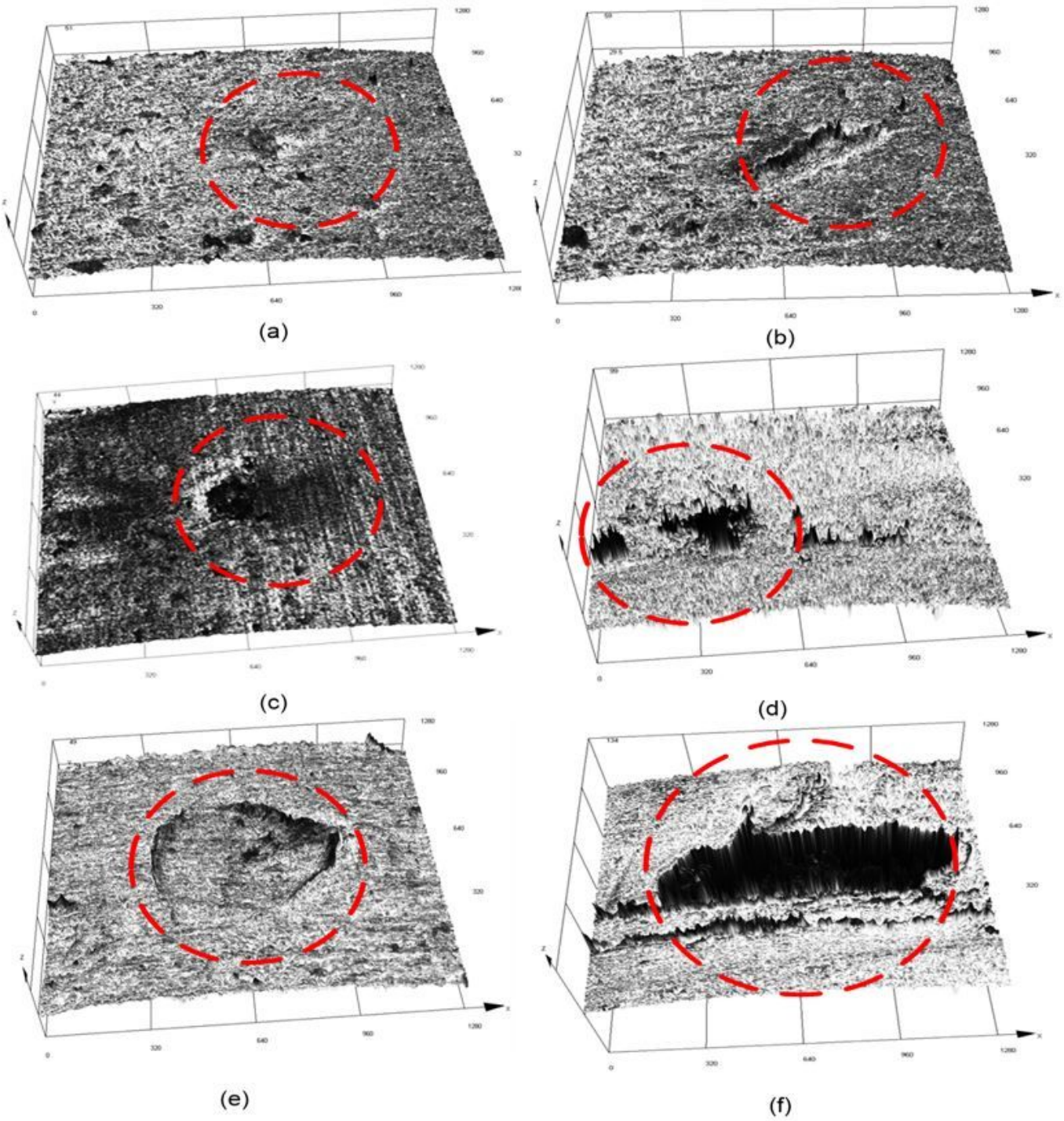

Figure 13

Surface topo graphs of inner race surfaces obtained in HL, EHL and BL regimes

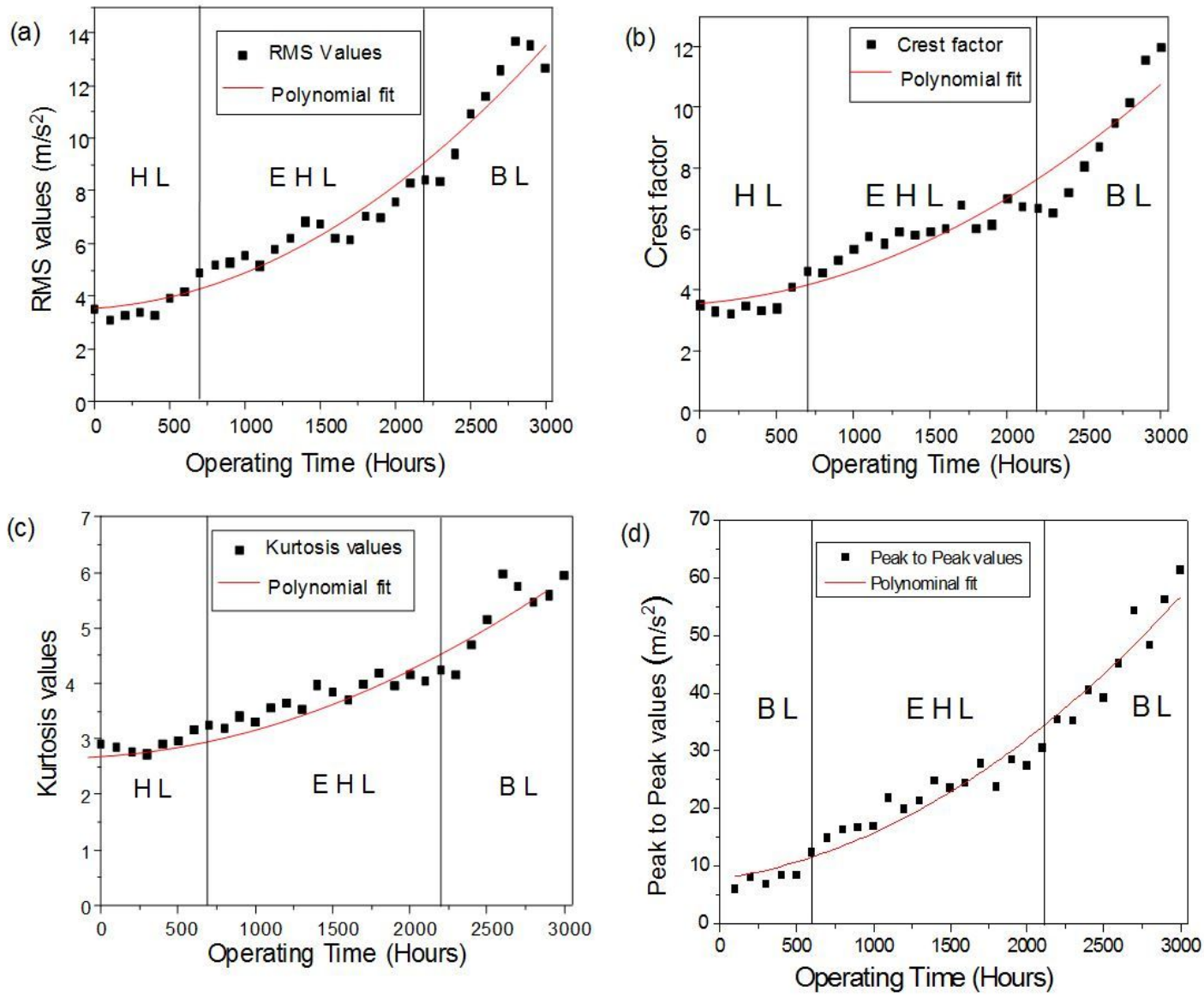

Figure 14

Statistical parameters of vibration signals w.r.t. operating time

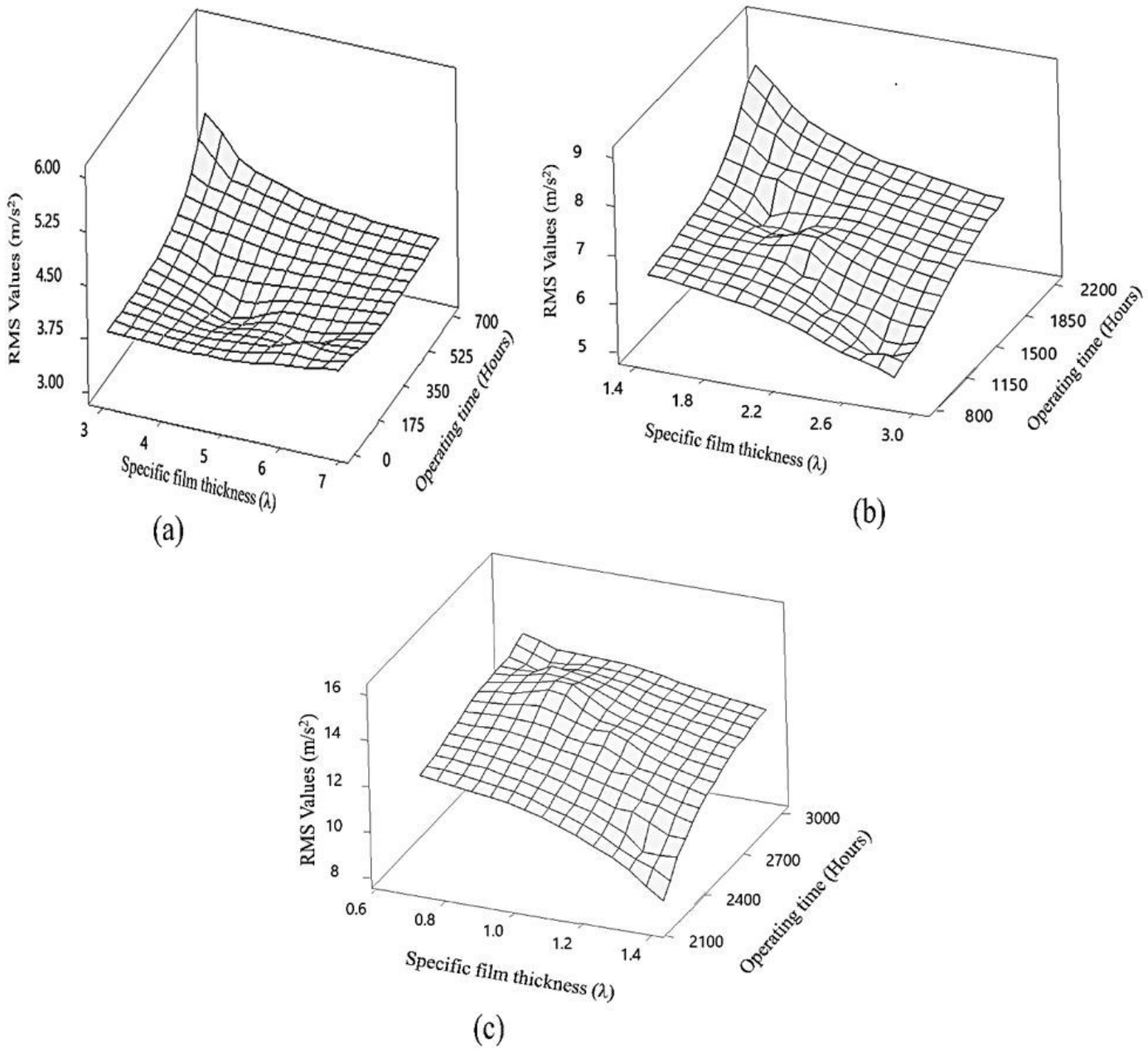

Figure 15

Effect of change in lubrication regimes on vibration signals (a) HL (b) EHL (c) BL

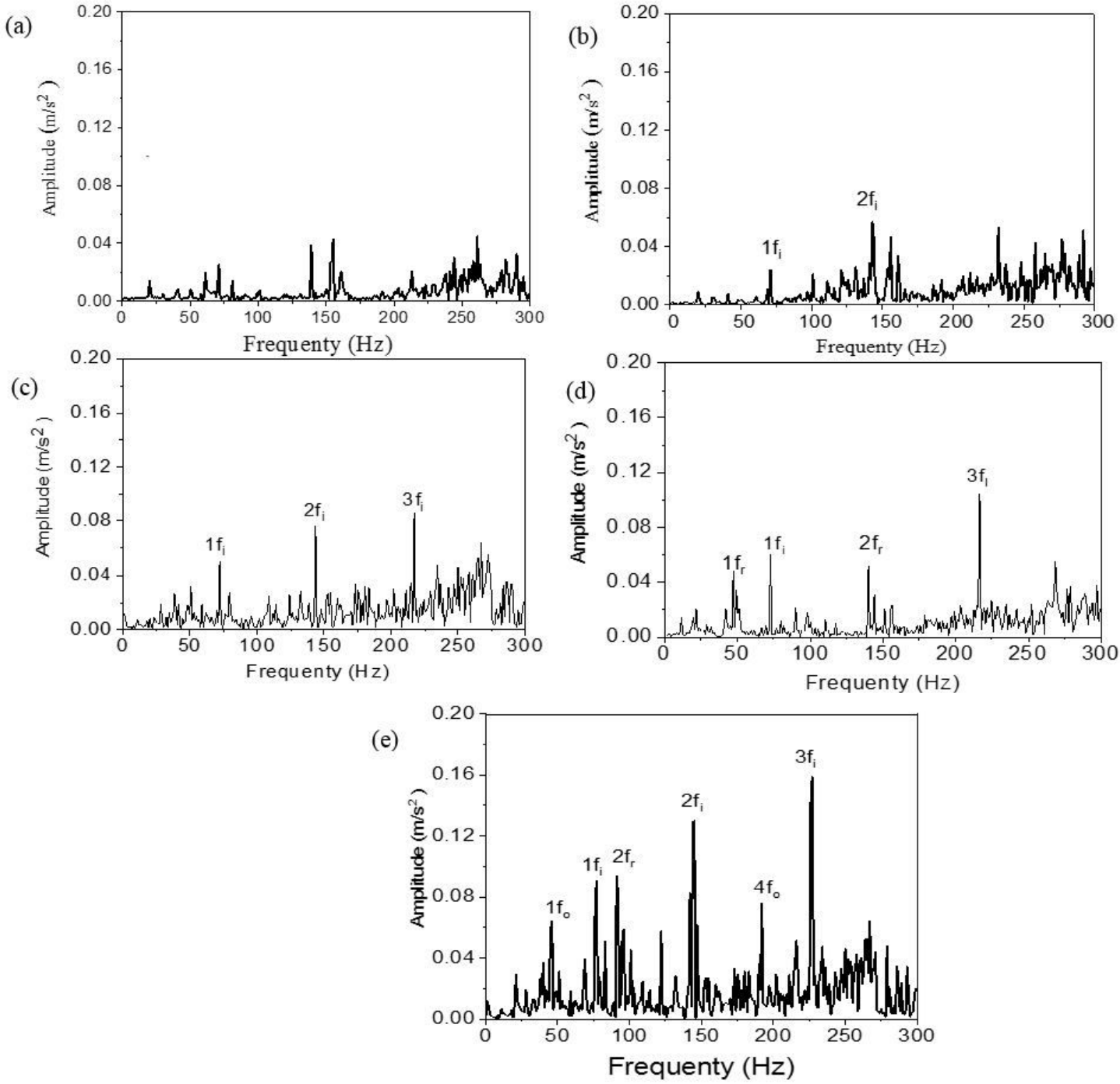

Figure 16

Fourier transform spectra of vibration signals (a) healthy bearing (b) 700 hours (c) 1500 hours (d) 2200 hours (e) 3000 hours